NASA Contractor Report 172270

THE MECHANICS OF DELAMINATION IN FIBER-REINFORCED COMPOSITE MATERIALS

Part II - Delamination Behavior and Fracture Mechanics Parameters

S. S. Wang and I. Choi

UNIVERSITY OF ILLINOIS
Urbana, Illinois 61801

Grant NAG1-286
November 1983

National Aeronautics and Space Administration

Langley Research Center
Hampton, Virginia 23665

THE MECHANICS OF DELAMINATION IN FIBER-REINFORCED COMPOSITE MATERIALS:

Part II - Delamination Behavior and Fracture Mechanics Parameters

by

S. S. Wang* and **I. Choi†**

Department of Theoretical and Applied Mechanics
University of Illinois
Urbana, IL 61801

---

*Associate Professor of Theoretical and Applied Mechanics

†Research Associate; Now with Xerox Corporation, Rochester, NY 14644

ABSTRACT

Based on theories of laminate anisotropic elasticity and interlaminar fracture, the complete solution structure associated with a composite delamination is determined. Fracture mechanics parameters characterizing the interlaminar crack behavior are defined from asymptotic stress solutions for delaminations with different crack-tip deformation configurations. A numerical method employing singular finite elements is developed to study delaminations in fiber composites with any arbitrary combinations of lamination, material, geometric, and crack variables. The special finite elements include the exact delamination stress singularity in its formulation. The method is shown to be computationall accurate and efficient, and operationally simple. To illustrate the basic nature of composite delamination, solutions are shown for edge-delaminated $[\theta/-\theta/-\theta/\theta]$ and $[(\pm\theta)/(\pm\theta)/90°/\overline{90°}]_s$ graphite-epoxy systems under uniform axial extension. Three-dimensional crack-tip stress intensity factors, associated energy release rates, and delamination crack-closure are determined for each individual case. The basic mechanics and mechanisms of composite delamination are studied, and fundamental characteristics unique to recently proposed tests for interlaminar fracture toughness of fiber composite laminates are examined. Influences of lamination, geometric, and crack variables on the delamination behavior are investigated.

1. INTRODUCTION

In an associate paper [1], the fundamental nature of stress singularity and asymptotic solution fields associated with a delamination between dissimilar anisotropic fiber composites have been studied. Lekhnitskii's complex-variable stress potentials [2] in conjunction with an eigenfunction expansion method have been used in the formulation and establishment of the general solution. The eigenvalues, especially the ones which characterize the strength of stress singularity, for delaminations with different local traction boundary conditions near the crack tip have been determined. Of particular interest are the asymptotic deformation and stress governing the composite delamination fracture. Since logarithmic terms are absent in the solutions for the delamination stress and deformation [1], the general structure of the complete solutions consists of only a power-type eigenfunction series of both singular and higher-order terms. The set of unknown constants in the eigenfunction series solution for a delamination problem can only be determined by solving the complete boundary-value problem with a full consideration of overall composite geometry, lamination and material variables, remote boundary conditions, and end loading conditions.

In a finite-dimensional fiber composite laminate with simple lamination variables and crack geometry, for example, a symmetric angle-ply $[\theta/-\theta/-\theta/\theta]$ composite containing edge delaminations along the θ and $-\theta$ ply interface, the complete laminate elasticity solution can be determined in an explicit form by the use of different analytical methods such as the boundary-collocation method [3]. However, for a composite laminate having more than four plies, the aforementioned collocation method is not applicable, and a more general and versatile method of approach to the problem is needed. The situation could become extremely complex for delaminations in a composite containing a

large number of plies with different fiber orientations and laminar thicknesses. The almost unlimited number of variables in a general composite delamination problem requires the development of an advanced analytical method which can not only deal with the local singular behavior of the delamination but also take into account various combinations of lamination, material, geometric, and crack variables. Numerical methods such as finite element methods are considered to be most attractive because of their versatility in handling mechanics problems with complex structural geometry and material properties. In this paper, the currently developed laminate elasticity solution is incorporated in the formulation of a set of conforming finite elements with singular derivative fields [4]. The special crack-tip elements are shown later to be particularly suitable for modeling the composite delamination problem. The use of laminate elasticity solutions derived from the associated paper [1] permits the inclusion of exact delamination stress singularities in finite element formulation, leading to extremely accurate and efficient numerical solutions for studying the fundamental behavior of composite delamination with complex lamination variables and geometric parameters.

Specific objectives of this paper are to: (1) establish complete solution structures for different delamination configurations to serve as a basis of formulating an advanced numerical method, (2) construct special crack elements of various kinds to model the composite delamination, (3) properly define interlaminar fracture mechanics parameters, e.g., stress intensity factors and energy release rates, for general composite laminates, (4) examine the fundamental behavior and associated characteristics of the composite delamination, and (5) assess influences of lamination, geometric and crack variables on the delamination response and composite failure modes.

In the next section, the general structure of complete solutions for delamination stress and displacement fields is given. Fracture mechanics parameters in terms of interlaminar crack-tip stress intensity factors and strain energy release rates are defined for various deformation modes of composite delamination. Special six-node, quasi three-dimensional crack elements for the present composite delamination problem are introduced in Section 3. Formulations of the singular elements and adjacent nonsingular eight-node isoparametric elements are briefly outlined. Solution strategy and computational scheme for the delamination problem, especially in the case that crack-surface closure (i.e. the contact problem) occurs, are discussed. Computational methods for evaluating stress intensity factors and energy release rates by using the singular finite elements are given in detail. In Section 4, solution accuracy and convergence are studied to demonstrate the efficiency and effectiveness of the present approach. The fundamental behavior and unique characteristics of composite delamination are examined in Section 5. Two graphite-epoxy laminate systems, i.e., symmetric angle-ply $[\theta/-\theta/-\theta/\theta]$ and symmetric $[(\pm\theta)/(\pm\theta)/90°/\overline{90°}]_s$ composites, with delaminations emanating from laminate edges are studied. Delamination crack-tip deformation and fracture mechanics parameters are determined for each case. Influences of fiber orientation, ply thickness, and crack size on delamination failure mechanics and mechanisms are investigated also.

2. COMPLETE SOLUTION AND FRACTURE MECHANICS PARAMETERS

2.1 Complete Solutions for Stress and Displacement

As discussed in the associated paper [1], the eigenvalues δ_n can be determined by solving the transcendental characteristic equation Eq. 20 in [1]. Depending upon the local crack-tip boundary conditions and the interface continuity conditions, the δ_n have the following values:

(i) delamination with open crack surfaces:

$$\delta_n = \begin{cases} n - 1/2 & \text{(single root)}, \\ n & \text{(triple roots)}, \\ (n - 1/2) \pm i\gamma & \text{(single root)}, \end{cases} \qquad (n = 0,1,2,\ldots\infty);$$

(ii) delamination with closed crack surfaces in frictionless contact

$$\delta_n = \begin{cases} n - 1/2 & \text{(double roots)}, \\ n & \text{(quadruple roots)}, \end{cases} \qquad (n = 0,1,2,\ldots\infty);$$

(iii) delamination with closed crack surfaces in frictional contact

$$\delta_n = \begin{cases} n - 1/2 & \text{(single root)}, \\ n - \beta & \text{(single root)}, \\ n & \text{(quadruple roots)}, \end{cases} \qquad (n = 0,1,2,\ldots\infty).$$

Once the values of δ_n are determined, the relationship among C_k's can be found and the complete solutions for displacement and stress can be established in explicit forms. For example, for a delamination with homogeneous local boundary conditions in a composite laminate subjected to planar loading, the complete solutions for stress and displacement components have the following expressions:

$$\sigma_i = \sum_{n=0}^{\infty} \Big(c_{1n} \sum_{k=1}^{3} \{ \mathrm{Re}[b_{kn}^{(1)} \Lambda_{ik} z_k^{n-1/2}] + \mathrm{Im}[b_{(k+3)n}^{(1)} \bar{\Lambda}_{ik} \bar{z}_k^{n-1/2}] \}$$

$$+ \sum_{k=1}^{3} \{ [c_{2n} b_{kn}^{(2)} + c_{3n} b_{kn}^{(3)}] \, \mathrm{Re}(\Lambda_{ik} z_k^n) + [c_{4n} b_{kn}^{(4)}] \, \mathrm{Im}(\Lambda_{ik} z_k^n) \}$$

$$+ \{ c_{5n} \mathrm{Re}[\sum_{k=1}^{6} b_{kn}^{(5)} \Lambda_{ik} z_k^{n-1/2+i\gamma}] + c_{6n} \mathrm{Im}[\sum_{k=1}^{6} b_{kn}^{(5)} \Lambda_{ik} z_k^{n-1/2+i\gamma}] \} \Big) + \sigma_{oi}$$

$$(i = 1,2,4,5,6), \qquad (1)$$

$$u_j = \sum_{n=0}^{\infty} \Big(c_{1n} \sum_{k=1}^{3} \{ \mathrm{Re}[b_{kn}^{(1)} \Gamma_{(j+3)k} z_k^{n+1/2}] + \mathrm{Im}[b_{(k+3)n}^{(1)} \bar{\Gamma}_{(j+3)k} \bar{z}_k^{n+1/2}] \} / (n+1/2)$$

$$+ \sum_{k=1}^{3} \{ [c_{2n} b_{kn}^{(2)} + c_{3n} b_{kn}^{(3)}] \mathrm{Re}[\Gamma_{(j+3)k} z_k^{n+1} / (n+1)] + c_{4n} b_{kn}^{(4)} \mathrm{Im}[\Gamma_{(j+3)k} z_k^{n+1} / (n+1)] \}$$

$$+ \{ c_{5n} \mathrm{Re}[\sum_{k=1}^{6} b_{kn}^{(5)} \Gamma_{(j+3)k} z_k^{n+1/2+i\gamma} / (n+1/2+i\gamma)]$$

$$+ c_{6n} \mathrm{Im}[\sum_{k=1}^{6} b_{kn}^{(5)} \Gamma_{(j+3)k} z_k^{n+1/2+i\gamma} / (n+1/2+i\gamma)] \} \Big) + u_{oj} \quad (j = 1,2,3), \qquad (2)$$

where $b_{kn}^{(\alpha)}$ are known eigenvectors corresponding to the unknowns $c_{\alpha n}$ for each given δ_n, and σ_{oi} and u_{oj} are known quantities from particular solutions for each individual case. We note that the $b_{kn}^{(\alpha)}$ are found to be the same for all δ_n's because of the involvement of the term $e^{in\phi}$ ($\phi = \pi$ and $-\pi$) in the $\underset{\sim}{D}(\delta_n)$ matrix. The constants Λ_{ik} and Γ_{ik} are defined as

$$\Lambda_{1k}= \mu_k^2,\quad \Lambda_{2k}= 1,\quad \Lambda_{4k}= -\eta_k,\quad \Lambda_{5k}= \mu_k\eta_k,\quad \Lambda_{6k}= -\mu_k;$$

$$\Gamma_{1k}= 1,\quad \Gamma_{2k}= \eta_k,\quad \Gamma_{3k}= \mu_k,\quad \Gamma_{4k}= p_k,\quad \Gamma_{5k}= q_k,\quad \Gamma_{6k}= t_k, \qquad (3)$$

where μ_k, η_k, p_k, q_k, t_k are related to ply stiffness matrix and can be found in [2,3]. The expressions for stresses and displacements for delamination with closed crack surfaces, i.e., nonvanishing local traction boundary conditions, can be easily determined to have forms similar to Eqs. 1 and 2 but with slight modifications owing to different numbers of algebraic multiplicity of the eigenvalues involved.

2.2 Delamination Stress Intensity Factors and Energy Release Rates

The stress and displacement fields for a delamination are shown in the preceding section to possess general form of Eqs. 1 and 2 with unknown constants $c_{\alpha n}$ to be determined. A proper analytical or numerical method with the aid of global laminate boundary conditions and remote loading conditions is required to determine the detailed solution for the complete boundary-value problem. Since the interlaminar fracture is controlled by local stress and deformation, the asymptotic solution is of primary importance and interest in understanding the near-field behavior and fracture phenomenon. The asymptotic solution is recognized to be singular in nature and governed by the delamination stress singularities, which have been obtained in detailed in [1]. As pointed out in the associated paper [1], the singular eigenvalues depend upon the local delamination configuration; thus, distinct structures of asymptotic solutions are obtained for different crack-tip deformations.

In general, the asymptotic solution for a delamination stress field can be written in the following form:

$$\sigma_i = \sum_{j=1}^{\ell} \sum_{k=1}^{3} [f_{ik}^{(j)} z_k^{\delta_j} + f_{i(k+3)}^{(j)} \bar{z}_k^{\delta_j}]$$

$$(i = 1,2,3,\ldots,6), \qquad (4)$$

where z_k and $\bar{z}_k$ have their origin located at the delamination tip. The $f_{ik}^{(j)}$ and $f_{i(k+3)}^{(j)}$ are functions of lamina material constants, lamination variables, and loading conditions. The integer ℓ is the total number of eigenvalues δ_j which satisfy the constraint condition,

$$-1 < \mathrm{Re}[\delta_j] < 0 \qquad (5)$$

For the convenience of further developments, Eq. 4 may be rewritten as

$$\sigma_i = \sum_{j=1}^{\ell} s_i^{(j)}(r,\phi;\ \delta_j), \qquad (6)$$

where $s_i^{(j)}$ is the jth component (corresponding to the eigenvalue δ_j) of the asymptotic stress σ_i in the polar coordinate system.

In view of the asymptotic solution structures given in Eq. 4 and those given in [1,5,6], it is possible to define, in the context of interlaminar fracture mechanics, the delamination stress intensity factors and strain energy release rates in a manner consistent with those for a homogeneous crack and for the refined model of an interface crack between dissimilar isotropic media [7,8]. For example, in the case of a closed delamination with crack surfaces in frictionless contact, the stress intensity factors can be introduced by considering the crack-tip interlaminar stresses σ_2, σ_6 and σ_4 (i.e., σ_y, τ_{xy}, τ_{yz}, or $\sigma_{\phi\phi}$, $\tau_{r\phi}$, $\tau_{z\phi}$) along the ply interface $\phi = 0$ as

$$K_I = \lim_{r\to 0^-} \sqrt{-2\pi r}\ \sigma_2(r,0) \tag{7a}$$

$$K_{II} = \lim_{r\to 0^+} \sqrt{2\pi r}\ \sigma_6(r,0) \tag{7b}$$

$$K_{III} = \lim_{r\to 0^+} \sqrt{2\pi r}\ \sigma_4(r,0) \tag{7c}$$

where $r = 0^-$ and 0^+ denote the positions infinitesmally behind and ahead of the crack tip, respectively, because the normal traction σ_2 is finite ahead of a closed crack tip where shear tractions σ_6 and σ_4 are singular.

The strain energy release rate, G, and its components G_i ($i = 1,2,3$) may be evaluated by using Irwin's virtual crack extension concept [9] as

$$\begin{aligned} G &= G_1 + G_2 + G_3 \\ &= \lim_{\delta a\to 0} \frac{1}{2\delta a} \int_0^{\delta a} \{\sigma_2(r,0)[u_2^{(m)}(\delta a - r,\pi) - u_2^{(m+1)}(\delta a - r,-\pi)] \\ &\quad + \sigma_6(r,0)[u_1^{(m)}(\delta a - r,\pi) - u_1^{(m+1)}(\delta a - r,-\pi)] \\ &\quad + \sigma_4(r,0)[u_3^{(m)}(\delta a - r,\pi) - u_3^{(m+1)}(\delta a - r,-\pi)]\}dr, \end{aligned} \tag{8}$$

where δa is the length of virtual crack extension. The interlaminar stresses, σ_2, σ_6, and σ_4, in Eq. 8 can be obtained from the asymptotic stress field such as Eq. 4. The corresponding displacements are also those of the asymptotic field equations discussed in the previous section. In terms of the delamination stress intensity solutions K_i, the G and G_i for a closed crack can be shown to have a simple expression as

$$G = G_2 + G_3 = \frac{\pi}{4}(A_2 K_{II} + A_3 K_{III}) \tag{9}$$

In Eq. 9, G_1 is identically zero because of the displacement continuity across the closed delamination surfaces,

$$u_2^{(m)}(r,\pi) - u_2^{(m+1)}(r,-\pi) = 0 \qquad -c < r < 0, \tag{10a}$$

and A_2 and A_3 are evaluated from [5] with

$$u_2^{(m)} - u_2^{(m+1)} = A_2\sqrt{2|\delta a - r|} \tag{10b}$$

$$u_3^{(m)} - u_3^{(m+1)} = A_3\sqrt{2|\delta a - r|} \tag{10c}$$

as $r \to 0^+$.

For a delamination with extremely small crack closure, the simplified model by taking the limiting case of a partially closed crack discussed in [5,6] is used. The stress intensity solutions K_{II} and K_{III} are the same as those given in Eqs. 7(b) and 7(c), but the K_I is defined at $r \to 0^+$ as

$$K_I = \lim_{r\to 0^+} \sqrt{2\pi r}\ \sigma_2(r,0). \tag{11}$$

And the corresponding strain energy release rates G and G_i, then, have the form,

$$G = G_1 + G_2 + G_3 = \frac{\pi}{4}(A_1K_I + A_2K_{II} + A_3K_{III}). \tag{12}$$

In the case that a fully opened delamination is assumed and the eigenfunction expansion series is used for the asymptotic solution, the delamination stress intensity factors are introduced as [3]

$$K_I = \lim_{r\to 0^+} \sum_{j=1}^{3} \sqrt{2\pi}\, r^{-\delta_j}\, s_2^{(j)}(r,0;\delta_j), \tag{13a}$$

$$K_{II} = \lim_{r\to 0^+} \sum_{j=1}^{3} \sqrt{2\pi}\, r^{-\delta_j}\, s_6^{(j)}(r,0;\delta_j), \tag{13b}$$

$$K_{III} = \lim_{r\to 0^+} \sum_{j=1}^{3} \sqrt{2\pi}\, r^{-\delta_j}\, s_4^{(j)}(r,0;\delta_j). \tag{13c}$$

We note that in this case exact integration in Eq. 8 can be carried out and the strain energy release rate, G, can be determined easily. However, individual components G_i can not be separated explicitly in the integration because of the complex mathematical structure of the asymptotic solutions. Other methods such as the hybrid singular finite element analysis [10,11] are needed to determine the values of individual G_i.

3. COMPUTATION OF FIELD SOLUTIONS AND FRACTURE MECHANICS PARAMETERS

We have thus far obtained the complete solutions for stress and displacement and the fracture mechanics parameters from the asymptotic solutions for each individual case. The unknown constants $c_{\alpha n}$ as well as K_I and G_I are to be determined by solving the complete boundary-value problem, involving remote loading conditions and global geometric and lamination parameters. Now consider a finite-width composite laminate containing delaminations under mechanical loading as shown in Fig. 1 in [1]. As mentioned in Section 1, several numerical methods could be used to determine the complete solution for the delamination problem in a finite dimensional laminate. Owing to the singular nature of the interlaminar crack, the complex structural geometry, and numerous lamination parameters involved, the special numerical method employing recently introduced conforming singular finite elements is an attractive approach to the current problem. In this approach, the exact delamination stress singularities can be included in the formulation of the special elements. Thus, the unknown constants associated with the asymptotic solution and the fracture mechanics parameters governing the delamination behavior can be evaluated conveniently with a high degree of accuracy and a fast rate of solution convergence.

3.1 Singular Crack-Tip Elements and Surrounding Nonsingular Elements

In this study, we generalize the formulation and concepts of the conforming singular elements originally introduced for homogeneous isotropic elasticity problems [4] to the present quasi three-dimensional, anisotropic composite delamination problem. Formulation of the singular elements is based on selection of shape functions and their derivatives containing the exact eigenvalues which meet the constraint condition Eq. 5 of stress singularity

derived from the aforementioned eigenfunction analysis for the composite delamination. Detailed discussion of the nature of the singular elements has been given in [4]. Only relationships relevant to the current development are given here.

Consider a six-node triangular element with three degrees of freedom per node and stress singularity at node 1 as shown in Fig. 1(a). The element has general rectilinear anisotropic material properties with elastic compliance S_{ij}. By a proper transformation, any point in the element defined in global Cartesian coordinates (x,y,z) can be referred to both local polar coordinates (r,ϕ,z) and triangular coordinates (ρ,ξ,z) with the origin located at node 1. Within the element, the displacement components $\underset{\sim}{u}$ are related to the nodal displacements $\underset{\sim}{q}$ by the interpolation (or shape) function $\underset{\sim}{N}_s$ as

$$\underset{\sim}{u} = \underset{\sim}{U}(x,y) + \underset{\sim}{u}_o \qquad \text{with} \quad \underset{\sim}{U} = \underset{\sim}{N}_s \, \underset{\sim}{q}, \tag{14a,b}$$

where $\underset{\sim}{u}_o$ are known quantities resulted from applied loading, and

$$\underset{\sim}{u}^T = \{ u_1, u_2, u_3\}, \qquad \underset{\sim}{u}_o^T = \{u_{o1}, u_{o2}, u_{o3}\}, \tag{15a}$$

$$\underset{\sim}{q}^T = \{q_1^{(1)}, q_2^{(1)}, q_3^{(1)}, q_1^{(2)}, q_2^{(2)}, q_3^{(2)}, \ldots\ldots, q_1^{(6)}, q_2^{(6)}, q_3^{(6)}\}, \tag{15b}$$

$$\underset{\sim}{N}_s = \underset{\sim}{N}_s (\rho, \xi; \delta_j), \tag{15c}$$

in which the superscript T denotes transpose of the associated column vector, and the number in the superscript parentheses in Eq. 15(b) refers to the associated nodal number of $\underset{\sim}{q}$. Explicit expressions of the shape function $\underset{\sim}{N}_s$, involving proper eigenvalues δ_j determined for each individual delamination problem from [1] and local coordinates, are given in Appendix 1. Equation 14(b) can be written in a more explicit form as follows:

$$\underset{\sim}{U} = \{\rho^{\delta_j+1} \underset{\sim}{M}(\xi) + \underset{\sim}{L}(\rho,\xi)\} \, \underset{\sim}{q}, \tag{16}$$

where $\underset{\sim}{L}(\rho,\xi)$ is the nonsingular polynomial part of $\underset{\sim}{N}_s(\rho,\xi;\delta_j)$, independent of the number and location of nodes along the 2-3 edge of the element. Using the minimum potential energy theorem and following the same procedure as the conventional displacement-based finite element formulation, we can construct the element stiffness matrix $\underset{\sim}{k}_s$ for the crack-tip element as

$$\underset{\sim}{k}_s = \iint_{A_s} \underset{\sim}{B}_s^T \underset{\sim}{C} \underset{\sim}{B}_s \, dA, \tag{17}$$

where $\underset{\sim}{C}$ is the material stiffness matrix, and $\underset{\sim}{B}_s$ has the form

$$\underset{\sim}{B}_s = \underset{\sim}{\partial}(\rho^{\delta_j+1} \underset{\sim}{M} + \underset{\sim}{L}). \tag{18}$$

In Eq. 18, the $\underset{\sim}{\partial}$ is a matrix differential operator. We remark that the shape function of the singular element is chosen such that the element conforms with a nonsingular quadratic element matched through the common element boundary (i.e., along edge 2-3), and with singular elements of the same formulation through boundaries 1-2 and 1-3.

The surrounding nonsingular elements used in this study are quasi three-dimensional, eight-node isoparametric elements [Fig. 1(b)] with 24 degrees of freedom (three D.O.F.'s per node). Formulation of the element stiffness matrix for the nonsingular element has been given in detail in [12,13]. The element stiffness matrix $\underset{\sim}{k}_r$ for the adjacent element can be shown as

$$\underset{\sim}{k}_r = \iint_{A_r} \underset{\sim}{B}_r^T \underset{\sim}{C} \underset{\sim}{B}_r \, dA, \tag{19}$$

where

$$\underset{\sim}{B}_r = \underset{\sim}{\partial} \underset{\sim}{N}_r. \tag{20}$$

The shape function $\underset{\sim}{N}_r$ for an eight-node, quasi three-dimensional isoparametric element has standard quadratic expressions which can be found in [12,13].

3.2 Solution Procedure and Iteration Scheme for Crack Closure

In the finite element discretization of the delaminated composite, the singular elements are placed in a ring form with the delamination tip as the common node (Fig. 2). The element stiffness matrices $\underset{\sim}{k}_s$ and $\underset{\sim}{k}_r$ are true stiffness matrices relating unknown nodal displacements to nodal force vectors. The standard procedure of the matrix-displacement method [14] can be used to assemble the global stiffness matrix $\underset{\sim}{K}$ and loading vector $\underset{\sim}{Q}$ leading to the relationship,

$$\underset{\sim}{K}\,\underset{\sim}{q} = \underset{\sim}{Q} + \underset{\sim}{Q}_o, \tag{21}$$

where $\underset{\sim}{Q}_o$ denotes the additional nodal force resulted from the applied strain ε_o, and the assemblage may be expressed symbolically by

$$\underset{\sim}{K} = \sum_{i=1}^{n_s} \underset{\sim}{k}_s^{(i)} + \sum_{j=1}^{n_r} \underset{\sim}{k}_r^{(j)}, \tag{22a}$$

$$\underset{\sim}{Q} = \sum_{i=1}^{n_s} \underset{\sim}{Q}_s^{(i)} + \sum_{j=1}^{n_r} \underset{\sim}{Q}_r^{(j)}, \tag{22b}$$

in which n_s and n_r are the total numbers of singular and nonsingular elements, respectively.

In actual numerical computation of a delamination problem, a finite length of crack closure is assumed first. The problem now becomes an elastic contact problem because a part of the local boundary conditions is not known and needs to be determined from the solution. Specifically, the following continuity conditions are required along the closed portion of the delamination, $-c \leq r \leq 0$:

$$[\sigma_2(r,\pi)] = 0, \tag{23a}$$

$$[u_2(r,\pi)] = 0, \tag{23b}$$

where the bracket [ ] denotes the jump of the associated quantity across the closed crack surfaces, e.g., $u_2^{(m+1)}(r,-\pi) - u_2^{(m)}(r,\pi) = 0$. Thus, we solve Eq. 21 in terms of unknown pressures along the closed crack surface and use Eq. 23(a) to determine the contact stress on this surface. To enforce the conditions Eqs. 23(a) and 23(b), the solution technique proposed by Francavilla and Zienkiewicz [15] for an elastic contact problem is employed. The numerical procedure involves an iteration scheme to determine crack closure length and contact stress along the delamination surface. If the solution is admissible, the contact stress so obtained must be in compression and the displacement field should have no overlapping or interpenetration outside the contact region. In the case that crack closure length is found to be extremely small, say, less than the order of $10^{-5} \sim 10^{-6}$ times crack length, the delamination is then assumed to be open, and the simplified model discussed in [1,5] and in the preceding sections in this paper is used. For the case of a delamination with finite-length crack closure, the detailed iterative algorithm for evaluating crack closure and contact stress is given in Appendix 2.

3.3 Computation of Delamination Stress Intensity Factors and Energy Release Rates

As mentioned in the preceding sections, the stress intensity factors and energy release rates for a delamination are evaluated from the asymptotic solution of interlaminar stresses σ_2, σ_6 and σ_4 (or σ_y, τ_{xy} and τ_{yz}) and the displacements u_i along the plane of the crack. For a finite dimensional composite laminate containing delaminations, the asymptotic stress and displacement can be conveniently determined by the aforementioned singular

finite element method. Along the delamination plane $\xi = \xi_o$, the near-field stress and displacement fields are approximated by using Eq. 16 and its derivatives as

$$\underset{\sim}{\sigma} \simeq \rho^{\delta}\, \underset{\sim}{R}(\xi_o;\delta)\, \underset{\sim}{q}, \tag{24a}$$

$$\underset{\sim}{u} \simeq \rho^{\delta+1}\, \underset{\sim}{M}(\xi_o)\, \underset{\sim}{q} + \underset{\sim}{u}_o, \tag{24b}$$

where $\underset{\sim}{R}(\xi_o;\delta)$ is a matrix of derivatives of the shape function $\underset{\sim}{M}$ and ply elastic constants, and the ρ and ξ_o are related to the global coordinates by a simple transformation given in Appendix 1.

For a partially closed delamination or a delamination with a very small size of crack-tip closure for which the simplified model with inverse square-root singularity is used, the stress intensity factors and strain energy release rates can be evaluated easily from the singular finite element results. Taking $\underset{\sim}{\sigma}$ and $\underset{\sim}{u}$ along the delamination crack plane $\xi_o = 0$ (i.e., $\phi_o = 0$) , we can write the asymptotic interlaminar stresses and displacements along the interface in simple expressions as

$$\sigma_i \simeq A_k\, r^{-1/2} \qquad \begin{array}{l}(i=2,\ k=1;\ i=6,\ k=2,\ \text{and}\\ \ i=4,\ k=3),\end{array} \tag{25a}$$

$$u_j \simeq B_k\, r^{1/2} + u_{oj} \qquad \begin{array}{l}(j=1,\ k=2;\ j=2,\ k=1,\ \text{and}\\ \ j=3,\ k=3),\end{array} \tag{25b}$$

where A_k and B_k are obtained from the corresponding components of $\underset{\sim}{R}(\xi_o;\delta)$ and $\underset{\sim}{M}(\xi_o)$ in Eqs. 24(a) and 24(b) by setting $\xi_o = 0$, and $\delta = -1/2$. Thus, the delamination stress intensity factors K_i can be easily determined by

$$K_i = \sqrt{2\pi}\, A_i \qquad (i=I,II,III), \tag{26}$$

The energy release rates can be determined in a manner similar to that for K_i through Eq. 8 as

$$G = G_1 + G_2 + G_3$$

$$= \lim_{\delta a \to 0} \frac{1}{2\delta a} \int_0^{\delta a} \{ \sum_{k=1}^{3} (A_k \, r^{-1/2}) [B_k (\delta a - r)^{1/2}] \} dr$$

$$= \lim_{\delta a \to 0} \frac{1}{2\delta a} \int_0^{\delta a} \sum_{k=1}^{3} A_k B_k \left(\frac{\delta a - r}{r}\right)^{1/2} dr. \tag{27a}$$

The term u_{oj} in Eq. 25(b) is not included, because it does not result in any contributions to G_I and G after integration. Integration of the singular integral Eq. 27(a) can be carried out explicitly without difficulty. Then the strain energy release rates have the form

$$G = \sum_{i=1}^{3} G_i = \frac{\pi}{4}(A_1 B_1 + A_2 B_2 + A_3 B_3). \tag{27b}$$

We remark here that each term in Eq. 27(b) corresponds to the individual G_i components and that for a delamination with finite crack closure, the first term in Eq. 27(b) is identically zero, i.e., $G_I = 0$, because of the continuity of displacement across the crack surface.

4. SOLUTION ACCURACY AND CONVERGENCE

To demonstrate the accuracy and efficiency of the present method of approach, a symmetric angle-ply [45°/-45°/-45°/45°] graphite-epoxy laminate containing edge delaminations along the 45°/-45° ply interace is considered. For simplicity and without loss of generality, the composite is assumed to be subjected to uniform axial strain $\varepsilon_z = \varepsilon_o$ along the z-axis and have a geometry of b/h = 8 and $h_1 = h_2 = h = 0.25$ inch and delaminations of length $a = 0.25$ inch emanating from the edges. Elastic ply properties of unidirectional high-modulus graphite-epoxy identical to those of Eq. 28 in [1] are used. Owing to the geometric and lamination symmetry, only a quarter of the cross sectional area needs to be considered. In finite element discretization of the continuum, twelve special crack-tip elements of identical size and shape (Fig. 2) are used to model the near-field response of the composite delamination. The crack-tip elements are embedded in the mesh of eight-node, quasi three-dimensional isoparametric elements. Local and overall mesh arrangements for the finite element analysis of the composite delamination are shown in Fig. 3. To study the accuracy and convergence of field solutions, the mesh near the crack tip is continuously refined by halving the lengths of equal sides of the singular elements (e.g., the sides OE and OF in Fig. 3).

Using the computational method and the solution scheme discussed in the preceding sections, numerical results are obtained for the convergence study. Significantly global crack closure with $c/a = 0.34$ is found for the delamination in the [45°/-45°/-45°/45°] graphite-epoxy under the uniform axial extension, resulting in a negative K_I and identically vanishing G_I. [The detailed nature of delamination closure and related problems will be discussed in the next section.] In Tables 1 and 2, delamination stress intensity factors and energy release rates associated with the finite-element mesh

refinement are shown for systemmatic reduction in crack-tip element size ($\Delta h/h$) and increase in the total number of elements. It can be seen clearly that stable and converged solutions for all K_I and G_I are obtainable, as the crack-tip element size becomes smaller than 0.1h and the associated total number of elements exceeds 100. As anticipated, the delamination stress intensity factors (Table 1) are sensitive to the size of the crack-tip elements owing to the localized nature of the singular domain. However, the strain energy release rates are relatively insensitive to the element size and mesh refinement (Table 2) because the G_I are related to the global structural response of the delaminated composite. Furthermore, the crack-closure length is also found to be insensitive to the mesh refinement in this case.

To assess the accuracy of the current solutions for the composite delamination with global crack closure is not trivial because no analytical and numerical solutions are available in the literature for comparison. The only analytical study, which may be used as a reference, deals with the delamination problem by assuming the crack surface being fully open and employing an eigenfunction expansion method with the aid of a boundary collocation technique [3]. In Fig. 4, stress intensity solutions determined by the present singular finite element method including the crack-closure consideration are presented as a function of delamination length in the [45°/-45°/-45°/45°] graphite-epoxy. The dominant stress intensity factor K_{III} determined for the partially closed composite delamination by the present approach is about 6 ~ 7% higher than the value for an open crack from the boundary collocation results. However, solutions for K_I obtained by using the two distinct models differ from each other both in sign and in magnitude. In the current singular finite element analysis of the delamination problem, K_I is found always to be negative owing to the aforementioned crack closure,

whereas K_I determined for an assumed open crack is positive. Values of K_{II} and G_2 determined by the two approached are both negligibly small. The strain energy release rates obtained for the delamination are given in Fig. 5. For the partially closed delamination determined by the present approach, G_1 is identically zero, whereas the value of $G_1/(10^6\varepsilon_o^2)$ from the assumed open crack model is of the order of 10^{-6}--a value much smaller than that of G_3, the dominant component of energy release rates. Despite the different nature at the crack tip in these two approaches, the values of G_3 differ only slightly from each other.

We remark that though mathematically rigorous, the solution obtained using the eigenfunction expansion method with the assumption of open crack surfaces is physically inadmissible because severe interpenetration of dissimilar materials is found in the oscillatory displacement solution near the crack tip. Thus, the present singular finite element approach with a partially closed crack consideration provides physically meaningful solutions with a high degree of efficiency and accuracy for general composite delamination problems.

5. THE FUNDAMENTAL BEHAVIOR AND CHARACTERISTICS OF COMPOSITE DELAMINATION

In the preceding sections, we have introduced the complete solution structure and defined the governing fracture mechanics parameters for the delamination problem. Special finite elements with singular derivatives have been formulated to model the near-field response of a delamination in a finite dimensional composite laminate. Solution convergence and accuracy have been affirmed in terms of computational parameters (e.g., the size of crack-tip elements, the degree of finite element discretization, etc.). Having established these basic mechanics theories and the numerical method, we now proceed to study the fundamental behavior and characteristics of delamination in fiber composites with general lamination and geometric variables.

Two fiber composite material systems are examined in this section: (1) symmetric angle-ply $[\pm\theta]_s$ graphite-epoxy laminates with edge delaminations between θ and $-\theta$ plies, and (2) symmetric $[(\pm\theta)/(\pm\theta)/90°/\overline{90°}]_s$ graphite-epoxy with edge delaminations between $-\theta$ and 90° plies. The symmetric angle-ply composite laminate system is selected because several unique delamination characteristics are observed, which can be used to illustrate most clearly the basic interlaminar fracture mechanics and failure modes. More importantly, some of the most fundamental nature of delamination fracture determined from the presently introduced physically admissible model and mathematically rigorous solutions are not observable in the previously obtained solutions which contain the inadmissible oscillatory stress and deformation [3,5]. The $[(\pm\theta)/(\pm\theta)/90°/\overline{90°}]_s$ graphite-epoxy system is studied also because this lamination system, especially the one with $[(\pm30°)/(\pm30°)/90°/\overline{90°}]_s$ fiber orientations, is currently being considered for use in the evaluation of interlaminar fracture toughness of composite materials under static and cyclic loading [16,17]. The ply elastic properties of high-modulus unidirectional

graphite-epoxy given in Eq. 28 of Ref. [1] are used in all computations. In the $[\theta/-\theta/-\theta/\theta]$ composites, the following lamination and geometric parameters are employed: $h_1 = h_2 = h = 0.25$ inch and $b/h = 8$, whereas in the $[(\pm\theta)/(\pm\theta)/90°/\overline{90°}]_s$ composite laminates, actual dimensions of unidirectional graphite-epoxy used in laboratory experiments [16,17] are taken, i.e., $h_1 = h_2 = \ldots = h_{11} = 0.0054$ inch and $b = 0.75$ inch. Moreover, in all cases studied in this paper the composite laminates are considered to be subjected to uniform axial extension $\varepsilon_z = \varepsilon_o$ along the z direction.

Since the interlaminar crack-tip deformation and fracture mechanisms are governed by the asymptotic field solutions, we shall examine the fundamental behavior and associated characteristics of composite delamination in terms of interlaminar fracture mechanics parameters, i.e., crack-tip stress intensities, strain energy release rates, and crack-surface closure.

5.1 Influence of Fiber Orientation

The behavior of a delamination in the relatively simple angle-ply $[\pm\theta]_s$ laminates is significantly influenced by the fiber orientation θ. Results obtained by using the iterative solution scheme in Section 3.2 reveal that the delamination always possesses a finite-length crack-tip closure. Assuming that the crack surface is in frictionless contact, we find that the closure length is global in general. For example, in the $[\pm\theta]_s$ graphite-epoxy with edge delaminations of length $a = 0.25$ inch, significant crack closure is found in each case studied (Table 3). The contact-zone size, c/a, varies from approximately two-tenths to more than one-third of total delamination length for θ ranging between 15° to 60°. The crack-tip closure results in a negative opening-mode stress intensity factor $K_I < 0$ and an identically vanishing energy release rate $G_1 = 0$, as shown in Tables 4 and 5. Thus, the delamination behavior in the $[\theta/-\theta/-\theta/\theta]$ composites is apparently governed by

interlaminar shear stresses and deformations. In Tables 4 and 5, the out-of-plane tearing-mode (mode III) stress intensity factor K_{III} and associated energy release rate G_3 are clearly the dominant ones controlling the delamination fracture. (The values of K_{III} and G_3 are several orders of magnitude higher than those of K_{II} and G_2.) Also, the composite with $\theta \approx 15°$ possesses the highest K_{III} and G_3 among all θ's studied. These results suggest that in symmetric angle-ply composites, delamination initiation and growth are more intimately associated with local interlaminar shear than transverse normal stress.

We reiterate that the solutions obtained here by the use of the present interlaminar crack-closure model and the rigorous mathematical (combined theoretical and numerical) approach are physically admissible and meaningful, as contrary to the previously obtained inadmissible, oscillatory solutions from an eigenfunction expansion approach with the assumption of a fully open crack.

In the more complex graphite-epoxy laminates with $[(\pm\theta)/(\pm\theta)/90°/\overline{90°}]_s$ ply orientations, delaminations are always observed to occur between the $-\theta$ and 90° plies [16,17]. Starting with the partially closed crack model and using the iterative solution scheme, we find that the closure length of a delamination is less than 10^{-6} inch. Thus, for this extremely small crack closure the simplified model with an inverse square-root stress singularity discussed in Section 4.3 of [1] and in [5,6] is employed. In Figs. 6 and 7, variations of stress intensities K_I and energy release rates G_I with fiber orientation θ are shown for a delamination of length $a = 0.5b$. The crack tip is apparently governed by the opening- and inplane shearing-mode stresses; the K_I and K_{II} are one order of magnitude higher than K_{III} for all θ's studied. The value of G_3 is vanishingly small in general, and G_1 and G_2 are three orders of magnitude higher than G_3 because of the extremely small value of

A_3. Note that values of G_1, G_2 and G_3 depend not only on K_i but also on A_i as indicated in Eqs. 12 and 27(b). [Unfortunately, an explicit relationship among A_i, ply elastic constants, lamination parameters, geometric, and loading variables needs to be determined numerically because of the complex algebra involved.] We remark that the maximum K_I and G_I appear at $\theta \approx 32.5°$ and the maximum K_{II} and G_2 occur at $\theta \approx 35°$ in the $[(\pm\theta)/(\pm\theta)/90°/\overline{90°}]_s$ graphite-epoxy system. The selection of $[(\pm30°)/(\pm30°)/90°/\overline{90°}]_s$ lamination in the recently proposed interlaminar fracture toughness tests [16,17] using edge-delamination composite specimens is therefore a proper choice.

5.2 Influence of Ply Thickness

The ply thickness is an important geometric variable in studying the delamination behavior of composites. Changing the laminar thickness in a laminate alters the lateral constraint of adjacent plies in the thickness direction and, thus, directly affects the interlaminar crack behavior. For illustration, fracture mechanics solutions for the [45°/-45°/-45°/45°] graphite-epoxy composites with several ply thicknesses are presented in this section. For simplicity and without introducing further complications, the laminate width 2b and thickness 2W as well as the delamination length a are kept constant as before, while variation of ply thicknesses h_1 and h_2 (with $h_1 + h_2 = W = 0.5$ inch) is considered.

As shown in Figs. 8-10, altering the ply thickness h_1/W has appreciable effects on the fundamental behavior of the delamination. For instance, when a thick outer 45° ply is used, say, $h_1/W > 0.8$, the entire delamination surface is in contact with the other (Fig. 10), leading to a negative K_I with $G_1 = 0$. Delamination fracture in this situation is governed by the tearing-mode stress intensity factor K_{III} and the associated energy release rate G_3 (Figs. 8 and 9). When equal ply thickness, i.e., $h_1 = h_2$, is used, the in-plane

shearing-mode stress intensity K_{II} and the energy release rate G_2 are about zero, and K_{III} has the maximum stress intensification. However, as the outer 45° ply becomes thin, e.g., $h_1 < 0.2W$, the surfaces of delamination are opened up, i.e., $c/a = 0$, as shown in Fig. 10. In this situation, contributions of K_I and K_{II} to the local failure become increasingly appreciable; K_{II} and K_{III} are of the same order of magnitude but G_2 and G_1 are still relatively small as compared to G_3. In the limiting case of $h_1/W \to 0$, the in-plane shear could become dominant to govern the delamination.

5.3 Influence of Interlaminar Crack Length

For the symmetric composite laminates with either $[\pm\theta]_s$ or $[(\pm\theta)/(\pm\theta)/90°/\overline{90°}]_s$ fiber orientations, the interlaminar crack-tip behavior is affected by the size of delamination. As discussed in Section 5.1, the delamination in the $[\theta/-\theta/-\theta/\theta]$ graphite-epoxy system has a global crack closure. Figure 11 reveals general characteristics of the crack closure in the delaminated [45°/-45°/-45°/45°] graphite-epoxy. Under a uniform axial strain ε_o, the crack closure increases monotonically with crack length until the delamination becomes about two-ply thicknesses. As the delamination extends further, the closure length approaches an asymptotic value of $c/h = 0.375$, indicating that crack growth is governed by the interlaminar shear τ_{yz} and the tearing-mode stress intensity factor K_{III}, as shown in Fig. 4. The values of τ_{xy}, K_{II} and G_2 are orders of magnitude smaller than those of τ_{yz}, K_{III} and G_3 (Figs. 4 and 5). Note again that crack closure occurs for all a/h's in the [45°/-45°/-45°/45°] graphite-epoxy, leading to an identically zero G_1 and negative opening-mode stress intensity factor $K_I < 0$. In the case of a very small delamination emanating from a free edge under rising load, the interlaminar crack is inherently unstable and extends rapidly to about one or two-ply thicknesses (i.e., the plateaus in Figs. 4 and 5) before stable growth

would occur. This phenomenon has been indeed observed in laboratory experiments of edge-delamination tests of $[(\pm 30°]/\pm(30°)/90°/\overline{90°}]_s$ T300-5208 graphite-epoxy composite laminates [16].

In the $[(\pm 30°)/(\pm 30°)/90°/\overline{90°}]_s$ graphite-epoxy containing delaminations between -30° and 90° plies, the delamination is found to be open all along the crack surface for any given a/h, as discussed in Section 5.1. The solutions for K_I and G_I as a function of delamination length a/b are given in Figs. 12 and 13. Also shown in Fig. 13 are the results reported in [16] by using a conventional nonsingular finite element method in conjunction with a virtual crack-closure scheme for calculating the strain energy rates [18]. The difference is very appreciable to warrant the necessity of using the advanced analytical and numerical technique for solving the delamination problem accurately. We observe that local delamination growth in the $[(\pm 30°)/(\pm 30°)/90°/\overline{90°}]_s$ graphite-epoxy is governed by an inherently three-dimensional mixed-mode fracture process because the simultaneous presence of significantly high values of K_I, K_{II} and K_{III} shown in Fig. 12. Owing to the vanishingly small A_3, the value of G_3 is found to be negligible in comparison with G_1 and G_2 (Fig. 13). We remark that in the limiting cas of a very small delamination crack (i.e., $a/h \to 0$), interactions occur between the delamination crack tip and the laminate edge, leading to a slightly higher value of K_{III} as shown in Fig. 12.

A salient feature shown in Figs. 4, 5 and 12, 13 is that the stress intensity factors K_I and energy release rates G_I become independent of the crack length a/h or a/b as the delamination extends beyond a few ply thicknesses. This unique feature has been observed and used in the experimental study of interlaminar fracture toughness of composite laminates

[16,17]. Provided that the K_I and G_I are accurately determined by appropriate methods such as the present one, the stress intensity factors and energy release rates associated with observed edge delamination initiation and growth may be useful for characterizing delamination fracture and interlaminar crack resistance of composite laminates.

6. SUMMARY AND CONCLUSIONS

General expressions of stress and deformation fields in a fiber composite laminate with delaminations have been obtained from presently developed anisotropic laminate elasticity theory and basic concepts of interlaminar fracture mechanics. Fracture mechanics parameters such as stress intensity factors and energy release rates for delaminations with different crack-tip deformation configurations are defined in a manner consistent with those for a homogeneous crack and for the refined model of an interface crack between dissimilar isotropic solids [7,8]. In finite-dimensional composite laminates with complex lamination and geometric variables, an advanced numerical method employing special singular crack-tip finite elements is developed for modeling the delamination. Exact delamination stress singularities obtained from the laminate elasticity solution are included in the crack-tip element formulation. Solution convergence and accuracy have been studied to ensure the validity of the results and to demonstrate the efficiency and effectiveness of the method. To illustrate the fundamental nature of composite delamination, numerical results are shown for the $[\theta/-\theta/-\theta/\theta]$ and $[(\pm\theta)/(\pm\theta)/90°/\overline{90°}]_s$ graphite-epoxy laminate systems containing edge delaminations under uniform axial extension. Fracture mechanics parameters and failure modes associated with the composite delamination are determined for each case. The basic mechanics and mechanisms of delamination are studied for the composites with different lamination and geometric variables and crack parameters. Based on the results obtained, the following conclusions may be reached:

(1) To study the fundamental mechanics of delamination in a composite laminate having a large number of plies with different fiber orientations, advanced numerical methods such as the present one are essential to take into account the crack-tip singularity and the large number of lamination, material, and geometric variables involved.

(2) In the crack-tip element formulation, the inclusion of delamination stress singularities determined from the laminate elasticity solution by using an eigenfunction expansion method leads to very accurate solutions with a rapid rate of convergence. This is particularly advantageous for studying delamination problems in composite laminates with complex lamination, geometric, and material variables.

(3) Since the singular eigenvalues and their algebraic multiplicity are different for different crack tip deformation configurations, the crack element formulation and solution strategy for each delamination problem need to be treated on an individual basis. Stress intensity solutions and energy release rates in each case should be evaluated in accordance with the appropriate delamination models given in Section 2.

(4) The state of stress and deformation in the vicinity of a delamination crack tip are three dimensional in general. The asymptotic solutions can not be determined accurately by using classical lamination theory nor by any approximate methods without including interlaminar stresses and the correct stress singularities associated with the delamination. The current laminate elasticity solution and associated numerical method provide accurate information on the singular nature of the crack tip and complete field solutions for the delamination problem.

(5) The singular delamination stress field may be characterized by the presently introduced interlaminar fracture mechanics parameters. Crack-tip stress intensity factors K_i and energy release rates G_i can be determined only by solving the complete boundary-value problem. In contrast to the singular eigenvalues which depend only on local boundary conditions and material properties of adjacent plies, the K_i and G_i are functions of all lamination and geometric parameters, remote loading conditions, and crack variables.

(6) Owing to the local nature of interlaminar fracture, the mechanics and mechanisms of delamination growth are governed by the crack-tip stress intensity factors. In angle-ply $[\theta/-\theta/-\theta/\theta]$ graphite-epoxy, crack-tip closure occurs and, thus, $K_I < 0$; delamination growth may be, therefore, more intimately related to interlaminar shear stresses and interface shear strength than the transverse normal stress. In the cases of $[(\pm\theta)/(\pm\theta)/90°/\overline{90°}]_s$ graphite-epoxy, crack surfaces are open and delamination growth is controlled by all of the three-dimensional, mixed-mode stress intensity factors, K_I, K_{II}, and K_{III}.

(7) While the K_i govern local deformation and delamination fracture, the G_i are related to the global structural response and less sensitive to the local deformation and fracture. For example, the total G and G_3 differ only slightly between the cases of a delamination with a closed and an open crack tip in the $[\theta/-\theta/-\theta/\theta]$ graphite-epoxy composite. Thus, K_i may provide a more sensitive measure and, thus, better fracture parameters than G_i for evaluating the composite delamination growth.

(8) Influences of lamination variables such as fiber orientation and ply thickness on the delamination behavior are significant. Changing fiber orientation generally alters failure modes appreciably. For instance, in $[(\pm\theta)/(\pm\theta)/90°/\overline{90°}]_s$ graphite-epoxy, the opening-mode (K_I) dominated

delamination fracture changes into a shearing-mode (K_{II}) controlled failure, as the θ becomes greater than 40°. Also, increasing ply thickness h_1/W in $[\theta/-\theta/-\theta/\theta]$ graphite-epoxy affects the failure mode from a shearing-dominated, open delamination fracture to a closed one.

(9) Stress intensity solutions and energy release rates appear to be independent of crack length during the growth of an edge delamination, as long as the crack exceeds a length of few ply thicknesses [3,19]. This unique feature in composite edge-delamination is being used for evaluating of interlaminar fracture toughness of fiber composite laminates [16,17], provided that the K_I and G_I can be calculated accurately by using advanced analytical methods such as the present one.

7. ACKNOWLEDGMENTS

The research work described in this paper was supported in part by National Aeronautics and Space Administration-Langley Research Center (NASA-LaRC), Hampton, VA under Grant NAG 1-286 to the University of Illinois at Urbana-Champaign. The authors are grateful to Drs. T. K. O'Brien and N. Johnston of NASA-LaRC for the support and fruitful discussion.

8. REFERENCES

[1] Wang, S. S. and Choi, I., "The Mechanics of Delamination in Fiber-Reinforced Composite Materials, Part I: Delamination Stress Singularities and Solution Structure," NASA CR-172269, November 1983.

[2] Lekhnitskii, S. G., *Theory of Elasticity of Anisotropic Elastic Body*, Holden-Day, Inc., San Francisco, CA, 1963.

[3] Wang, S. S., "Edge Delamination in Angle-Ply Composite Laminates," NASA Contract Report NASA-CR-165439, NASA-Lewis Research Center, Cleveland, OH, 1981; also in *AIAA Journal*, Vol. 21, No. 11, 1983.

[4] Stern, M., "Families of Consistent Conforming Elements with Singular Derivative Fields," *International Journal for Numerical Methods in Engineering*, Vol. 14, 1979, pp. 409-421.

[5] Wang, S. S. and Choi, I., "The Interface Crack between Dissimilar Anisotropic Composite Materials," *ASME Journal of Applied Mechanics*, Vol. 50, 1983, pp. 169-178.

[6] Wang, S. S. and Choi, I., "The Interface Crack Behavior in Dissimilar Anisotropic Composites under Mixed-Mode Loading," *ASME Journal of Applied Mechanics*, Vol. 50, 1983, pp. 178-183.

[7] Comninou, M., "The Interface Crack," *ASME Journal of Applied Mechanics*, Vol. 44, No. 4, 1977, pp. 631-636.

[8] Comninou, M., "The Interface Crack in a Shear Field," *ASME Journal of Applied Mechanics*, Vol. 45, No. 2, 1978, pp. 287-290.

[9] Irwin, G. R., "Analysis of Stresses and Strains Near the End of a Crack Traversing a Plate," *ASME Journal of Applied Mechanics*, Vol. 24, 1957, pp. 361-364.

[10] Wang, S. S. and Yuan, F. G., "A Hybrid Finite Element Approach to Composite Laminate Elasticity Problems with Singularities," ASME Paper No. 83-WA/APM-15, *ASME Journal of Applied Mechanics*, Vol. 50, No. 4, 1983.

[11] Wang, S. S. and Yuan, F. G., "A Singular Hybrid Finite Element Analysis of Boundary-Layer Stresses in Composite Laminates," *International Journal of Solids and Structures*, Vol. 19, No. 9, 1983, pp. 825-837.

[12] Wang, S. S. and Stango, R. J., "Optimally Discretized Finite Elements for Boundary-Layer Stresses in Composite Laminates," *AIAA Journal*, Vol. 21, No. 4, 1983, pp. 614-620.

[13] Stango, R. J. and Wang, S. S., "Process-Induced Residual Thermal Stresses in Advanced Fiber Composite Laminates," in *Polymer Processing: Analysis and Innovation*, N. P. Suh and C. L. Tucker, III, Eds., ASME PED-Vol. 5, American Society of Mechanical Engineers, New York, 1982, pp. 67-81.

[14] Zienkiewicz, O. C., *The Finite Element Method*, Third Edition, McGraw-Hill, London, 1977.

[15] Francavilla, A. and Zienkiewicz, O. C., "A Note on Numerical Computation of Elastic Contact Problems," *International Journal for Numerical Methods in Engineering*, Vol. 9, 1975, pp. 913-924.

[16] O'Brien, T. K., "Characterization of Delamination Onset and Growth in a Composite Laminate," *Damage in Composite Materials, ASTM STP 775*, K. L. Reifsnider, Ed., American Society for Testing and Materials, 1982, pp. 140-167.

[17] O'Brien, T. K.; Johnston, N. J.; Morris, D. H.; and Simonds, R. A., "A Simple Test for the Interlaminar Fracture Toughness of Composites," *SAMPE Journal*, Vol. 18, No. 4, July/August 1982, pp. 8-15.

[18] Rybicki, E. F., Schmueser, D. W. and Fox, J., "An Energy Release Rate Approach for Stable Crack Growth in the Free-Edge Delamination Problem," *Journal of Composite Materials*," Vol. 11, 1977, pp. 470-482.

[19] Wang, S. S., "Fracture Mechanics for Delamination Problems in Composite Laminates," *Journal of Composite Materials*, Vol. 17, No. 3, 1983, pp. 210-223.

TABLE 1

Delamination Stress Intensity Factors K_i † Associated with Finite-Element Mesh Refinement in [45°/-45°/-45°/45°] Graphite-Epoxy

No. of Elements	Element Size (Δh/h)	K_I *	K_{II}	K_{III}
72	0.25	-0.6458E-1	0.3424E-2	-0.7114E 0
84	0.125	-0.6219E-1	0.2463E-2	-0.6967E 0
96	0.0625	-0.6141E-1	0.1796E-2	-0.6894E 0
108	0.03125	-0.6152E-1	0.1401E-2	-0.6855E 0

†K_i are normalized by $10^6\varepsilon_o$ (psi-$\sqrt{\text{in}}$).

*Closed crack tip with $c/a = 0.34$.

TABLE 2

Delamination Energy Release Rates G_i[†] Associated with Finite-Element Mesh Refinement in [45°/-45°/-45°/45°] Graphite-Epoxy

No. of Elements	Element Size ($\Delta h/h$)	G_1[*]	G_2	G_3
72	0.25	0.	0.6855E-6	0.1533E 0
84	0.125	0.	0.5528E-6	0.1519E 0
96	0.0625	0.	0.4619E-6	0.1512E 0
108	0.03125	0.	0.3943E-6	0.1508E 0

[†] G_i are normalized by $10^6\varepsilon_o^2$ (lb-in/in^2).

[*] Closed crack tip with $c/a = 0.34$

TABLE 3

Influence of Fiber Orientation on Crack-Tip Closure Length* for a Delamination in [θ/-θ/-θ/θ] Graphite-Epoxy Composite†

θ	c/a
0°	0.0
15°	0.2292
30°	0.2834
45°	0.3402
60°	0.3603

†$h_1 = h_2 = 0.25$ in., b = 2 in.; $a = 0.25$ in.

*at strain $\varepsilon_o = 10^{-6}$

TABLE 4

Effects of Fiber Orientations on Stress Intensity Solutions* for Delamination in [θ/-θ/-θ/θ] Graphite-Epoxy Composite†

θ	K_I	K_{II}	K_{III}
0°	0.	0.	0.
15°	-0.3782E-1	0.3866E-2	-0.2379E 1
30°	-0.1072E 0	0.8744E-2	-0.1943E 1
45°	-0.6152E 0	0.1401E-2	-0.6855E 0
60°	-0.8599E-2	0.2034E-3	-0.9270E-1

†$h_1 = h_2 = 0.25$ in., b = 2.0 in.; $a = 0.25$ in.

*K_i are scaled by $10^6 \varepsilon_o$ [psi-$\sqrt{\text{in}}$].

TABLE 5

Effects of Fiber Orientation on Strain Energy Release Rates[*] for a Delamination in [θ/-θ/-θ/θ] Graphite-Epoxy Composite[†]

θ	G_1[††]	G_2	G_3
0°	0.	0.0	0.0
15°	0.	0.6059E-5	0.2111E 1
30°	0.	0.2748E-4	0.1074E 1
45°	0.	0.3943E-6	0.1508E 0
60°	0.	0.1425E-7	0.3597E-2

[†] $h_1 = h_2 = 0.25$ in., b = 2 in.; a = 0.25 in.

[*] G_i are scaled by $(10^6 \varepsilon_o^2)$ [lb-in/in^2].

[††] G_1 is identically zero due to crack-tip closure.

9. LIST OF FIGURE CAPTIONS

Fig. 1 (a) Six-Node Quasi Three-Dimensional Crack-Tip Element with Singular Derivatives; (b) Eight-Node Quasi Three-Dimensional (nonsingular) Isoparametric Element.

Fig. 2 Arrangement of Special Crack-Tip Elements for the Composite Delamination Problem.

Fig. 3 Overall and Local Crack-Tip Finite-Element Mesh Arrangements for Modeling Delamination in [45°/-45°/-45°/45°] Graphite-Epoxy Composite.

Fig. 4 Comparison of Stress Intensity Solutions Obtained by Two Different Models/Approaches for Delamination in [45°/-45°/-45°/45°] Graphite-Epoxy Subjected to Uniform Axial Strain $\varepsilon_z = \varepsilon_o$ ($h_1 = h_2 = h = 0.25$ in., $b/h = 8$ in., $a = 0.25$ in.).

Fig. 5 Comparison of Energy Release Rates Determined by Two Different Models/Approaches for Delamination in [45°/-45°/-45°/45°] Graphite-Epoxy Subjected to Uniform Axial Strain $\varepsilon_z = \varepsilon_o$ ($h_1 = h_2 = h = 0.25$ in., $b/h = 8$, $a = 0.25$ in.).

Fig. 6 Variation of Stress Intensity Factors K_i with Fiber Orientation θ for Delamination in $[(\pm\theta)/(\pm\theta)/90°/\overline{90°}]_s$ Graphite-Epoxy under Uniform Axial Strain $\varepsilon_z = \varepsilon_o$ ($h_1 = h_2 = \ldots = h_{11} = 0.0054$ in., $b = 0.75$ in., $a = 0.5b$).

Fig. 7 Variation of Strain Energy Release Rates G_i with Fiber Orientations θ for Delamination in $[(\pm\theta)/(\pm\theta)/90°/\overline{90°}]_s$ Graphite-Epoxy under Uniform Axial Strain $\varepsilon_z = \varepsilon_o$ ($h_1 = h_2 = \ldots = h_{11} = 0.0054$ in., $b = 0.75$ in., $a = 0.5b$).

Fig. 8 Influence of Ply Thickness h_1/W on Stress Intensity Factors for Delamination in [45°/-45°/-45°/45°] Graphite-Epoxy Subjected to Uniform Axial Strain $\varepsilon_z = \varepsilon_o$ ($h_1 + h_2 = W = 0.5$ in., $2b/W = 8$, $a = 0.25$ in.).

Fig. 9 Influence of Ply Thickness h_1/W on Energy Release Rates G_i for Delamination in [45°/-45°/-45°/45°] Graphite-Epoxy Subjected to Uniform Axial Strain, $\varepsilon_z = \varepsilon_o$ ($h_1 + h_2 = W = 0.5$ in., $2b/W = 8$, $a = 0.25$ in.).

Fig. 10 Crack-Tip Closure Length as a Function of Ply Thickness h_1/W for Delamination in [45°/-45°/-45°/45°] Graphite-Epoxy Subjected to Uniform Axial Strain $\varepsilon_z = \varepsilon_o$ ($h_1 + h_2 = W = 0.5$ in., $2b/W = 8$, $a = 0.25$ in.).

Fig. 11 Crack-Tip Closure Length c/h as a Function of Delamination Size a/h in [45°/-45°/-45°/45°] Graphite-Epoxy Subjected to Uniform Axial Strain $\varepsilon_z = \varepsilon_o$ ($h_1 = h_2 = h = 0.25$ in., $b/h = 8$, $a = 0.25$ in.).

Fig. 12 Change of Stress Intensity Solutions K_i with Delamination Length a/b in $[(\pm 30°)/(\pm 30°)/90°/\overline{90°}]_s$ Graphite-Epoxy Subjected to Uniform Axial Strain $\varepsilon_z = \varepsilon_o$ ($h_1 = h_2 = \ldots = h_{11} = 0.0054$ in., $b = 0.75$ in.).

Fig. 13 Change of Strain Energy Release Rates G_i with Delamination Length a/b in $[(\pm 30°)/(\pm 30°)/90°/\overline{90°}]_s$ Graphite-Epoxy Subjected to Uniform Axial Strain $\varepsilon_z = \varepsilon_o$ ($h_1 = h_2 = \ldots = h_{11} = 0.0054$ in., $b = 0.75$ in.).

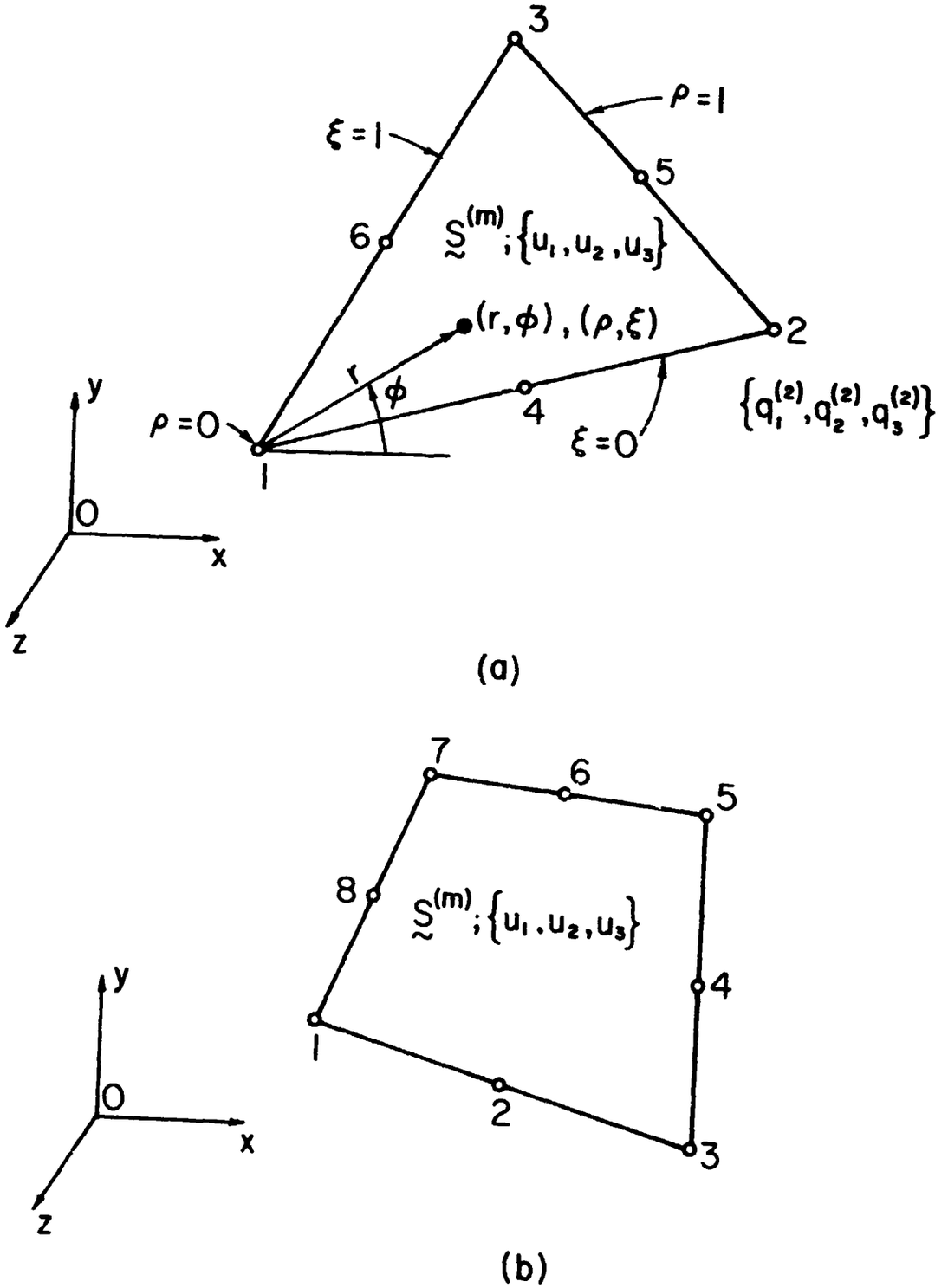

Fig. 1 (a) Six-Node Quasi Three-Dimensional Crack-Tip Element with Singular Derivatives; (b) Eight-Node Quasi Three-Dimensional (nonsingular) Isoparametric Element.

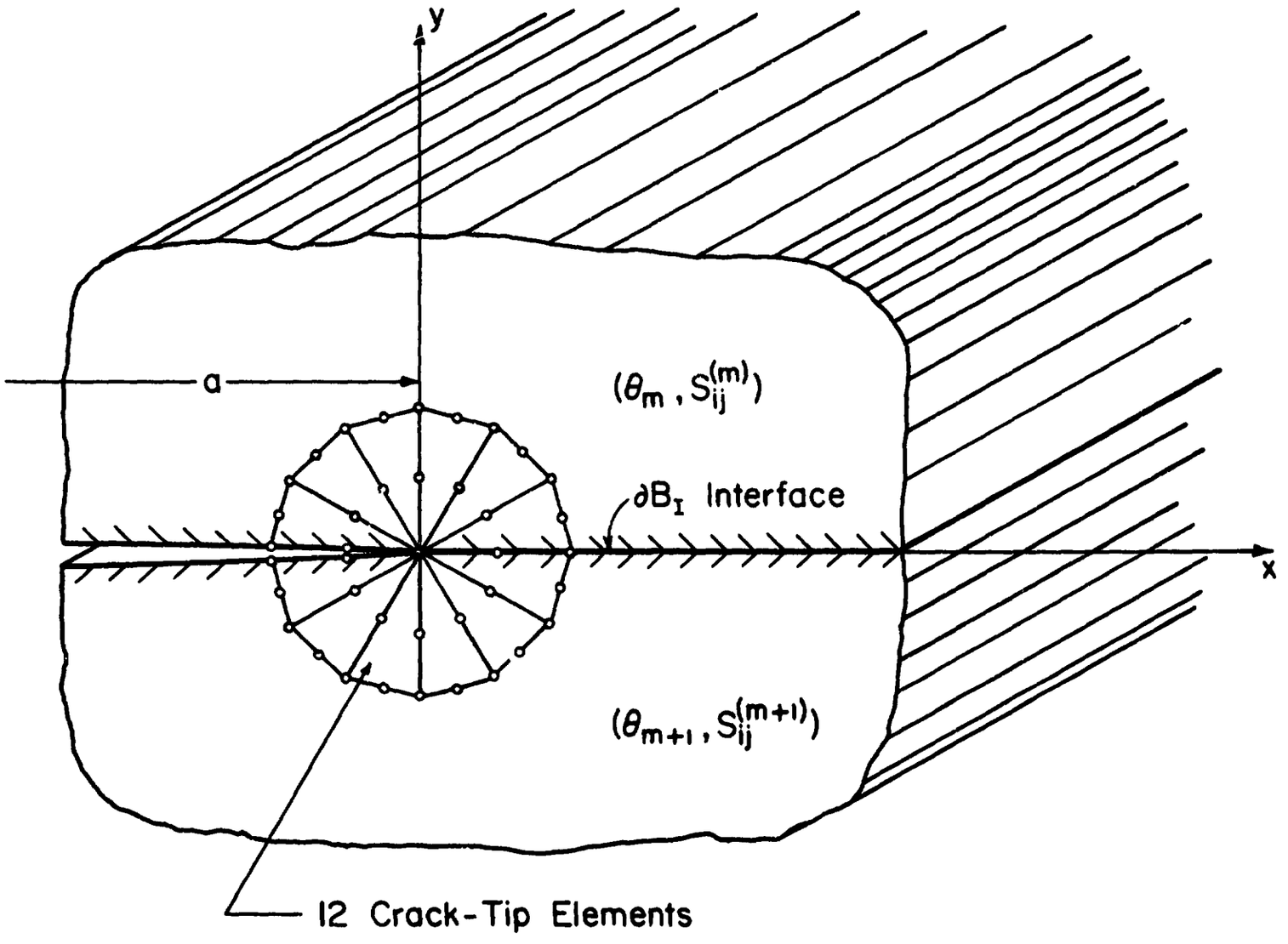

Fig. 2 Arrangement of Special Crack-Tip Elements for the Composite Delamination Problem.

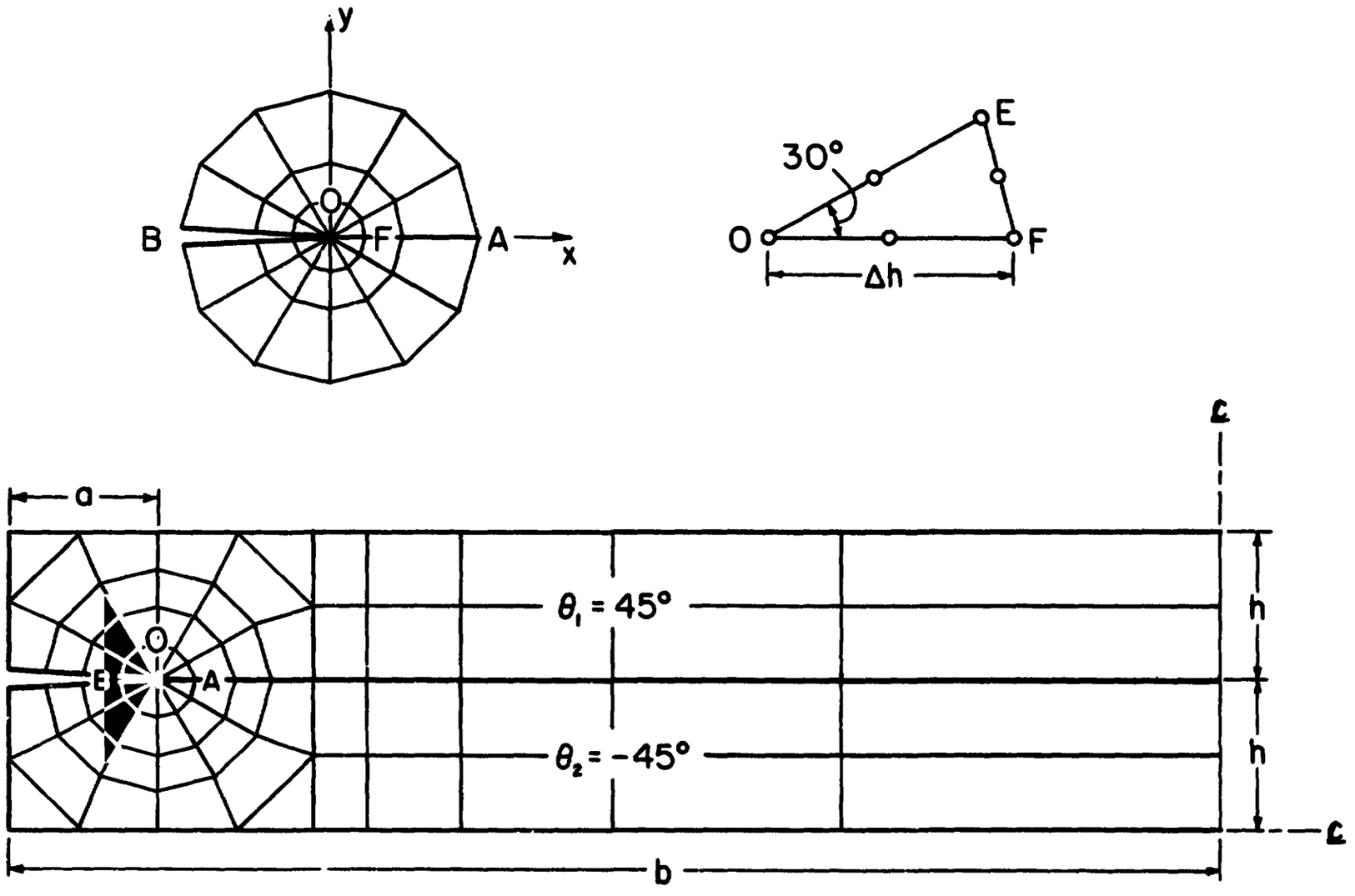

Fig. 3 Overall and Local Crack-Tip Finite-Element Mesh Arrangements for Modeling Delamination in [45°/-45°/-45°/45°] Graphite-Epoxy Composite.

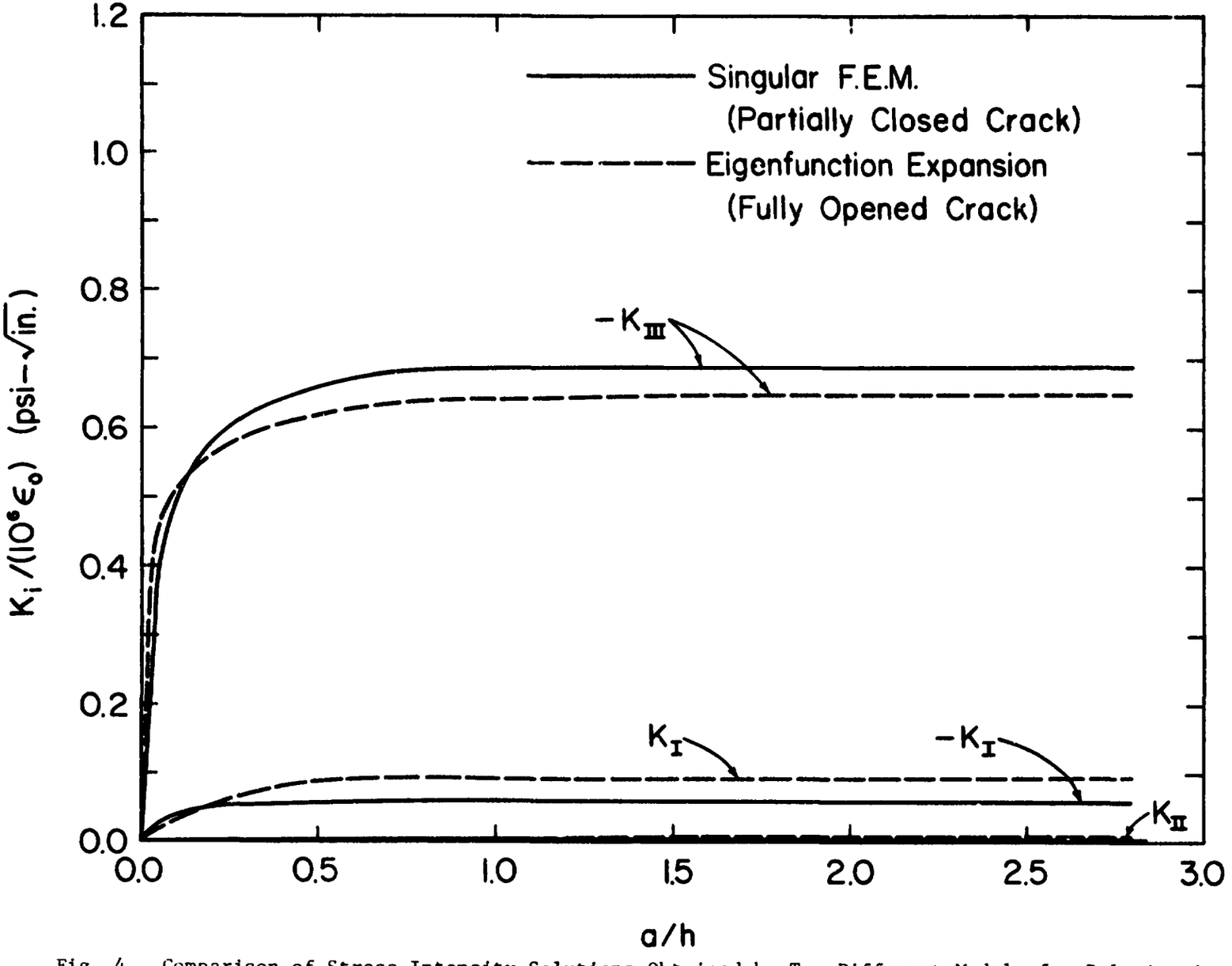

Fig. 4 Comparison of Stress Intensity Solutions Obtained by Two Different Models for Delamination in [45°/-45°/-45°/45°] Graphite-Epoxy Subjected to Uniform Axial Strain $\varepsilon_z = \varepsilon_o$ ($h_1 = h_2 = h = 0.25$ in., b/h = 8 in., $a = 0.25$ in.).

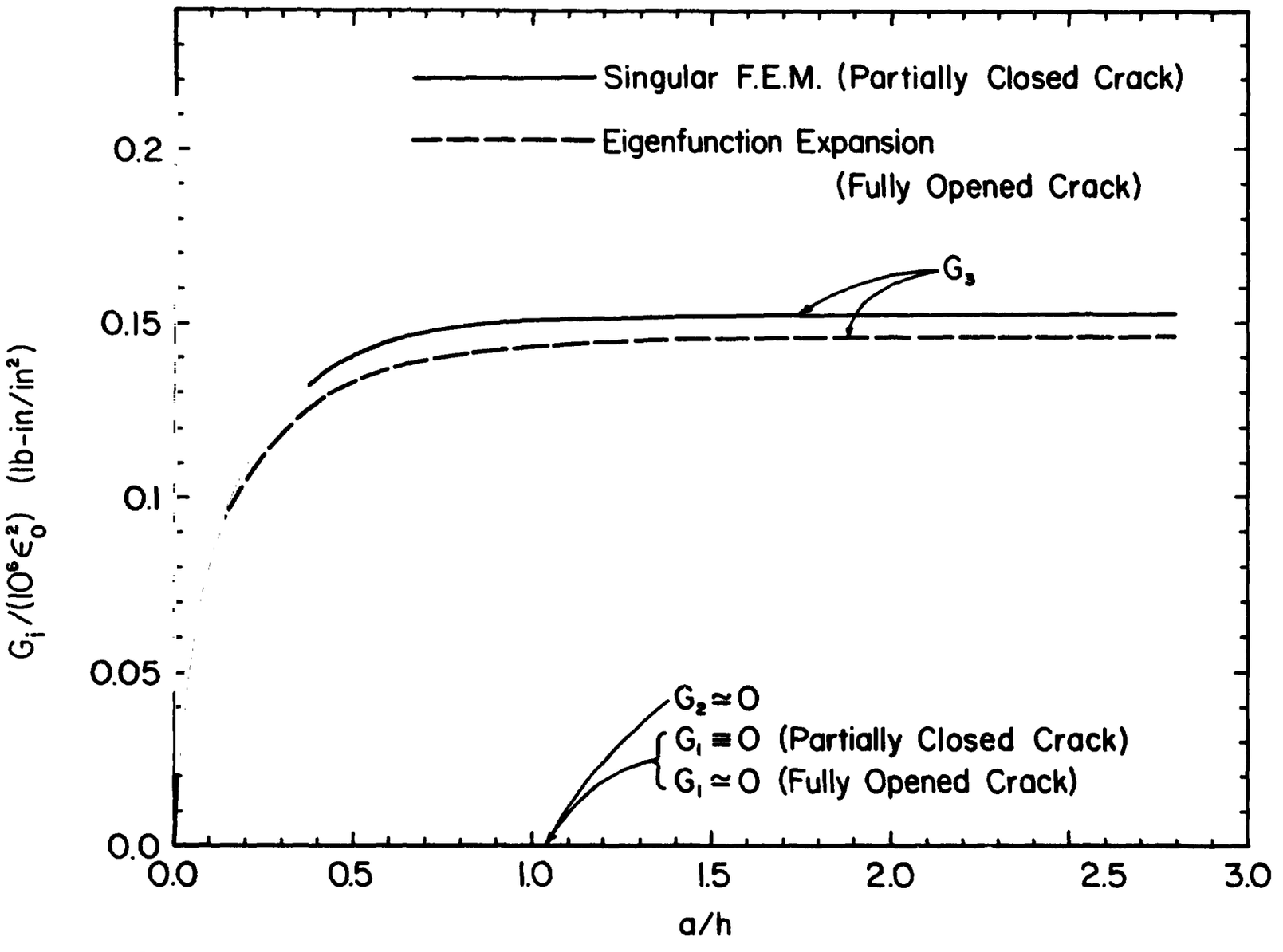

Fig. 5 Comparison of Energy Release Rates Determined by Two Different Models for Delamination in [45°/-45°/-45°/45°] Graphite-Epoxy Subjected to Uniform Axial Strain $\epsilon_z = \epsilon_o$ ($h_1 = h_2 = h =$ 0.25 in., b/h = 8, a = 0.25 in.).

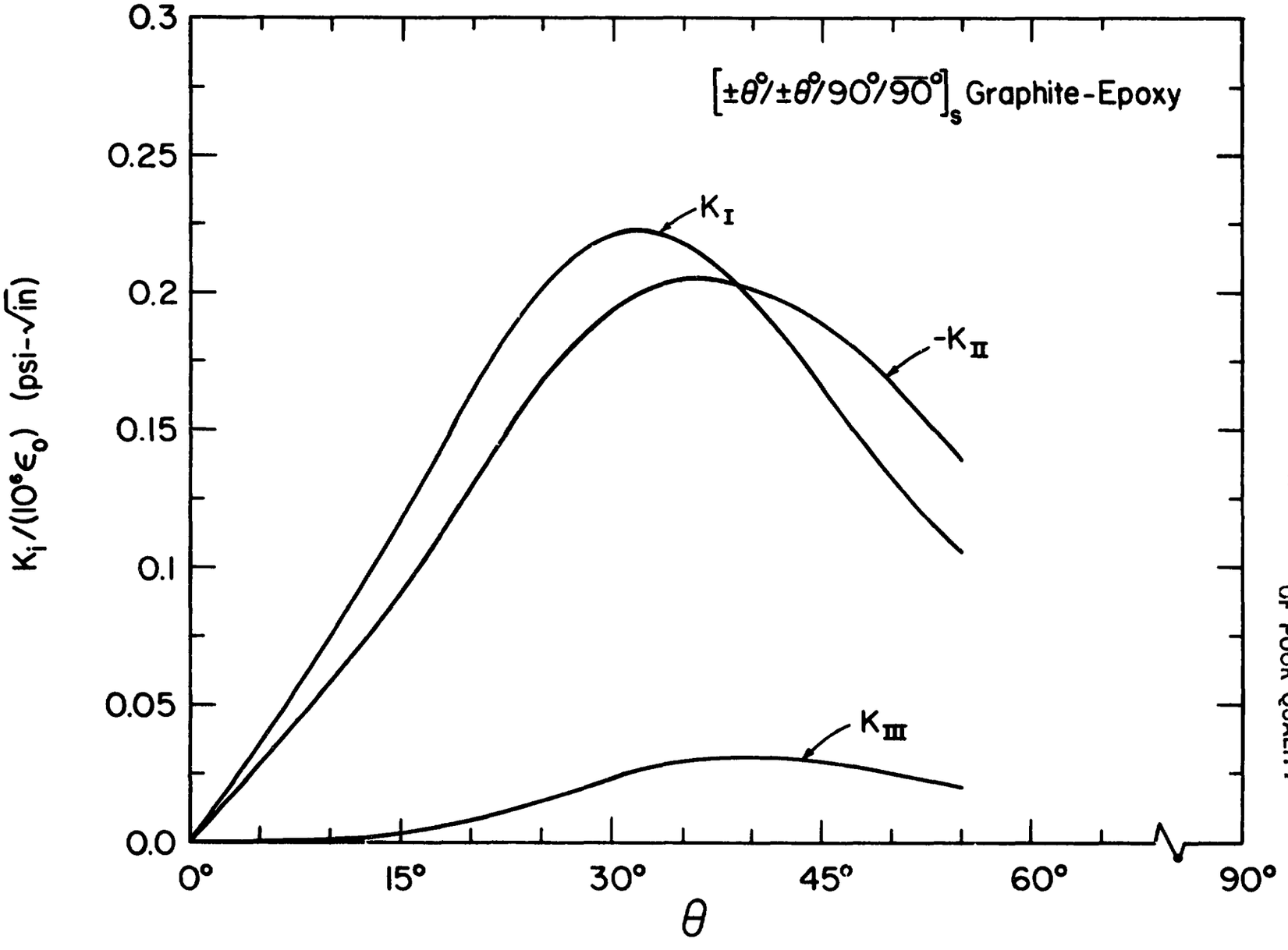

Fig. 6 Variation of Stress Intensity Factors K_i with Fiber Orientation θ for Delamination in $[(\pm\theta)/(\pm\theta)/90^\circ/\overline{90^\circ}]_s$ Graphite-Epoxy under Uniform Axial Strain $\varepsilon_z = \varepsilon_o$ ($h_1 = h_2 = \ldots = h_{11} = 0.0054$ in., b = 0.75 in., a = 0.5b).

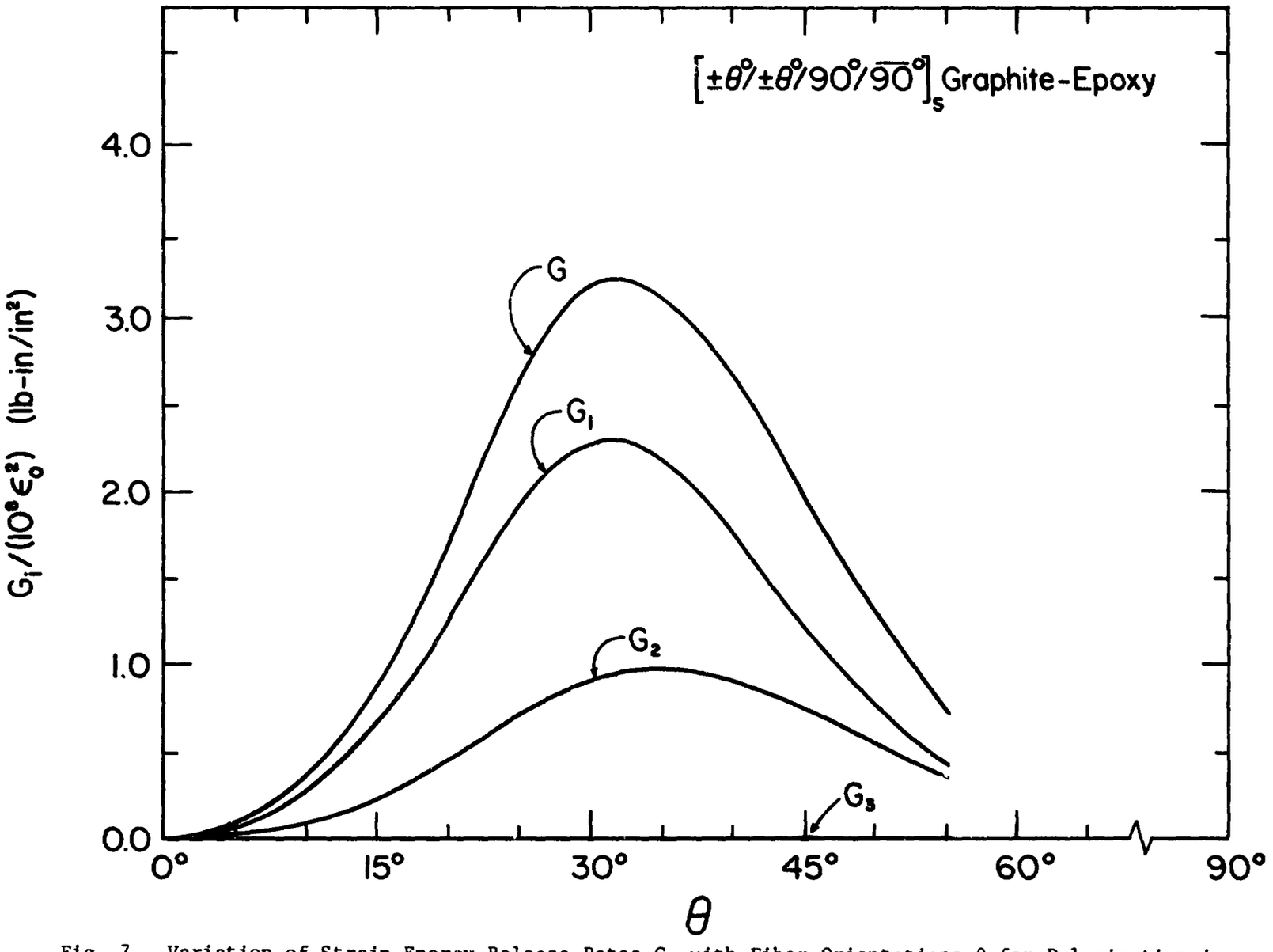

Fig. 7 Variation of Strain Energy Release Rates G_i with Fiber Orientations θ for Delamination in $[(\pm\theta)/(\pm\theta)/90^\circ/\overline{90^\circ}]_s$ Graphite-Epoxy under Uniform Axial Strain $\varepsilon_z = \varepsilon_o$ ($h_1 = h_2 = \ldots = h_{11} = 0.0054$ in., $b = 0.75$ in., $a = 0.5b$).

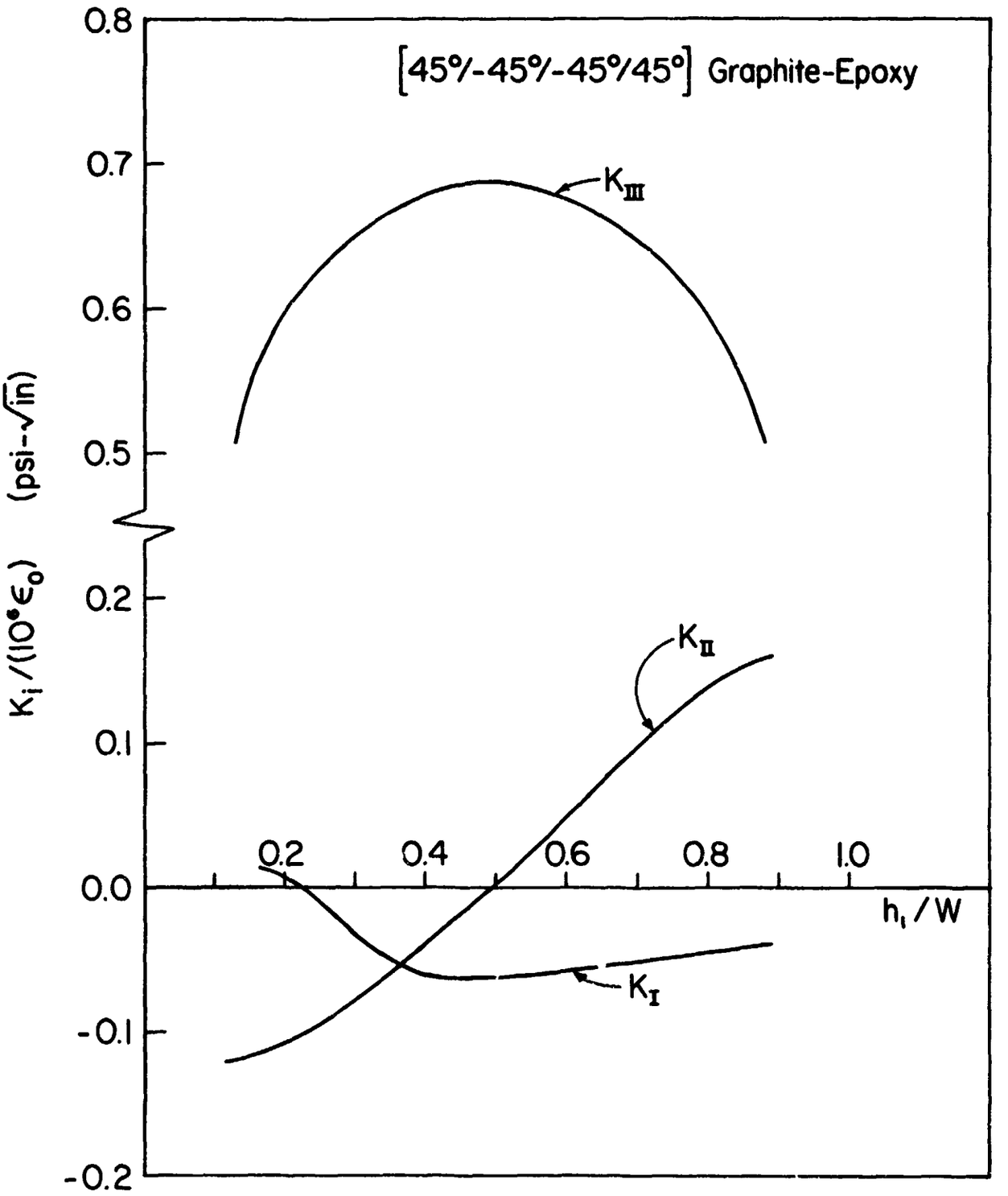

Fig. 8 Influence of Ply Thickness h_1/W on Stress Intensity Factors for Delamination in [45°/-45°/-45°/45°] Graphite-Epoxy Subjected to Uniform Axial Strain $\varepsilon_z = \varepsilon_o$ ($h_1 + h_2 = W = 0.5$ in., $2b/W = 8$, $a = 0.25$ in.).

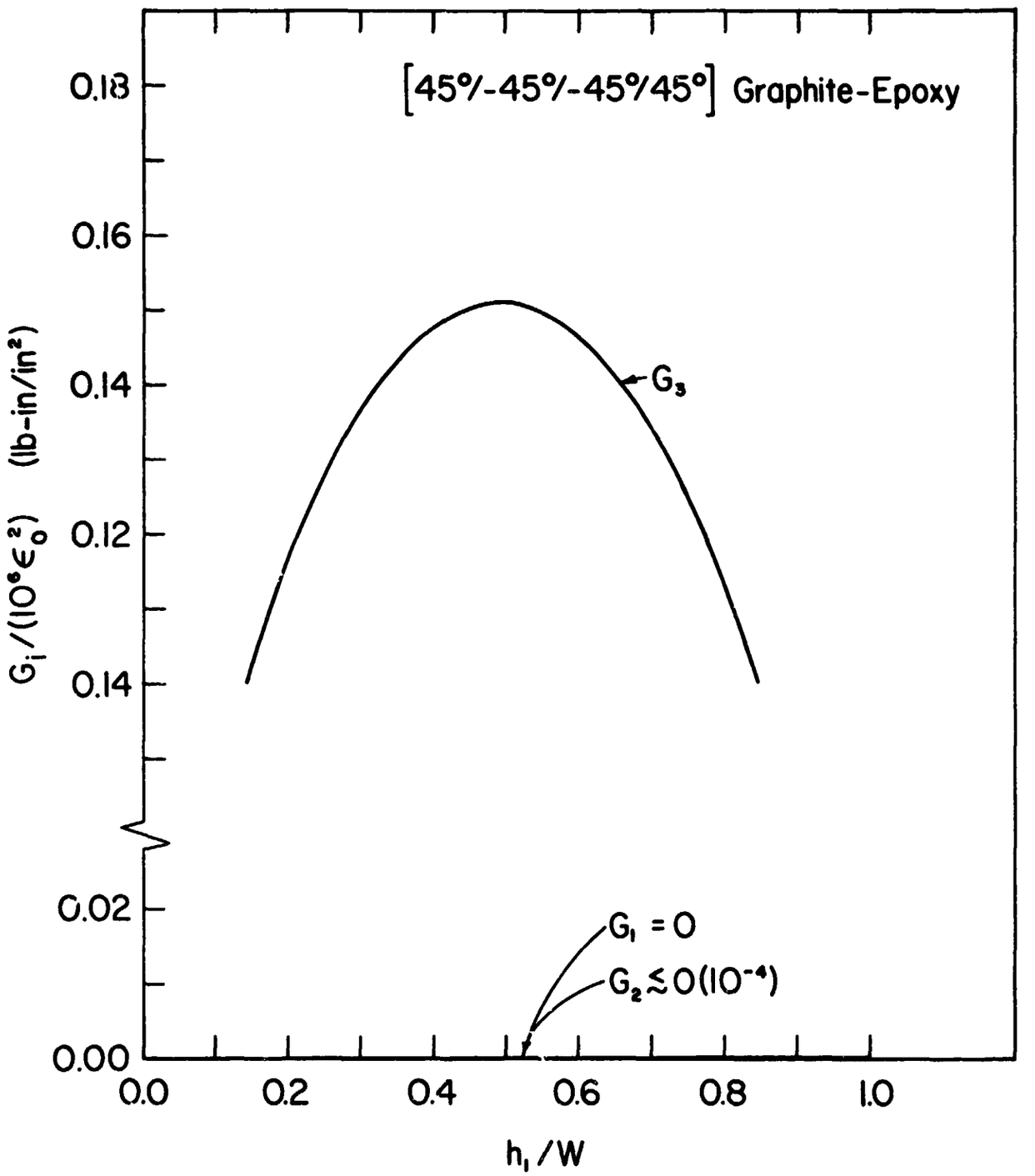

Fig. 9 Influence of Ply Thickness h_1/W on Energy Release Rates G_i for Delamination in [45°/-45°/-45°/45°] Graphite-Epoxy Subjected to Uniform Axial Strain, $\epsilon_z = \epsilon_o$ ($h_1 + h_2 = W = 0.5$ in., $2b/W = 8$, $a = 0.25$ in.).

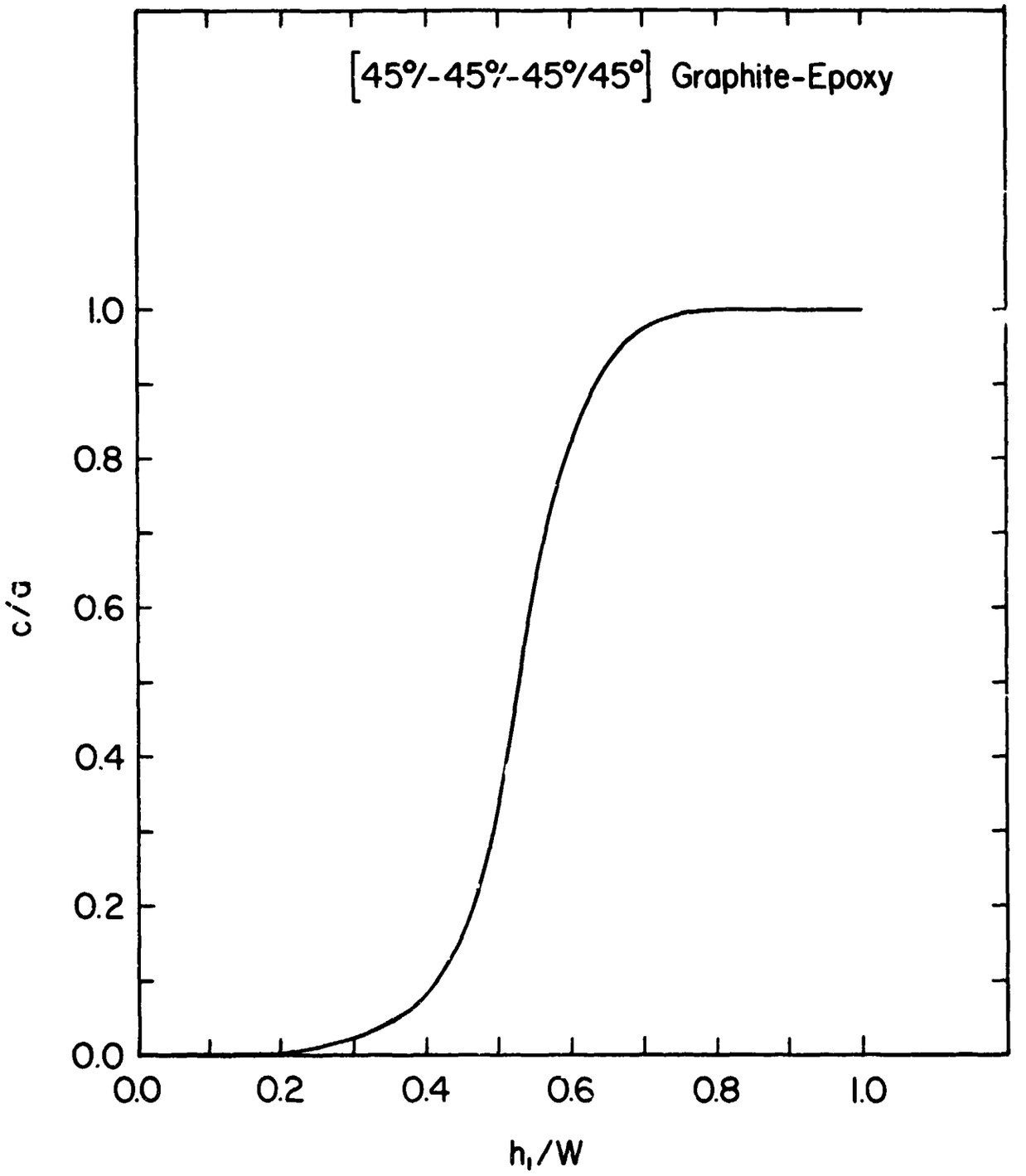

Fig. 10 Crack-Tip Closure Length as a Function of Ply Thickness h_1/W for Delamination in [45°/-45°/-45°/45°] Graphite-Epoxy Subjected to Uniform Axial Strain $\varepsilon_z = \varepsilon_o$ ($h_1 + h_2 = W = 0.5$ in., $2b/W = 8$, $a = 0.25$ in.).

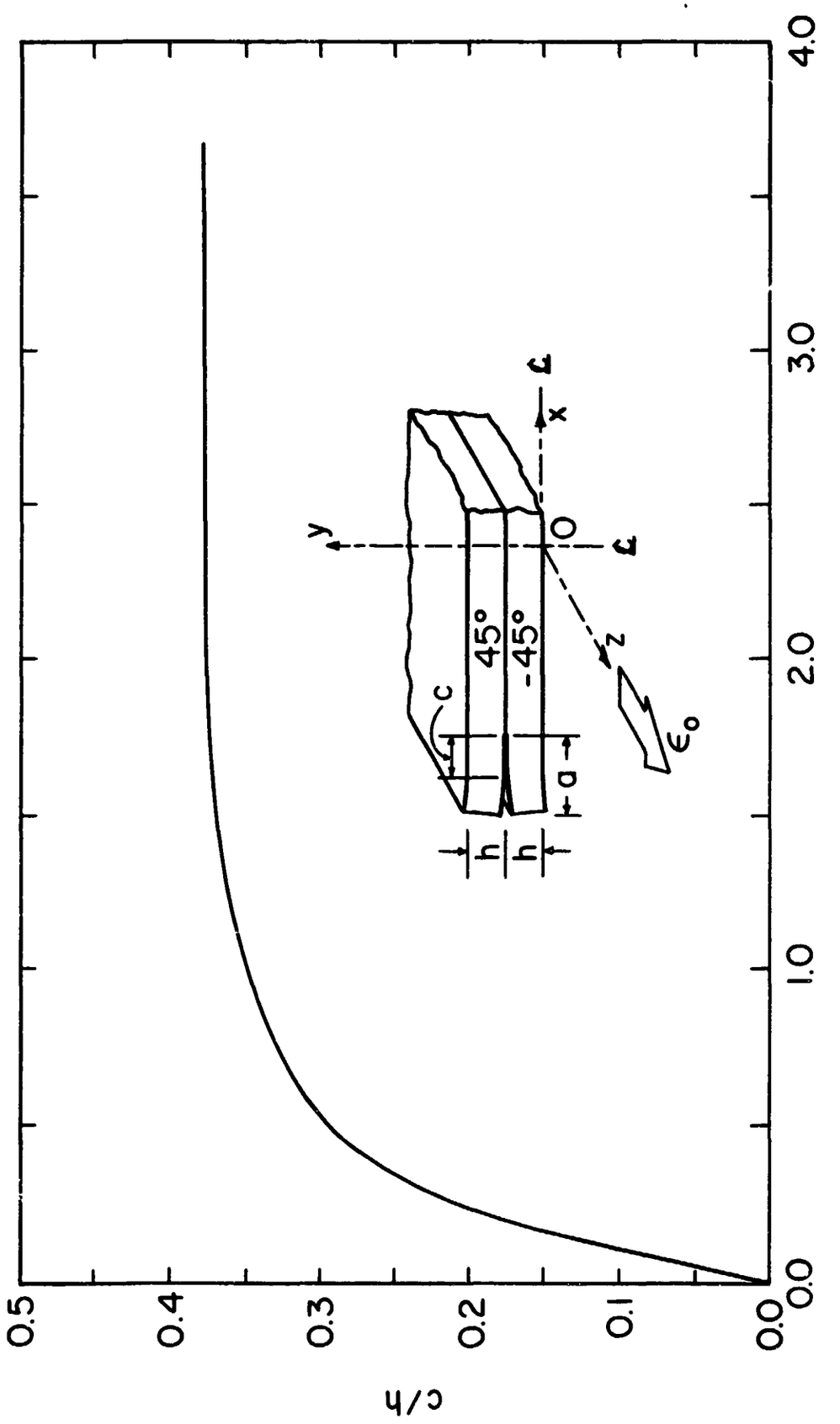

Fig. 11 Crack-Tip Closure Length c/h as a Function of Delamination Size a/h in [45°/-45°/-45°/45°] Graphite-Epoxy Subjected to Uniform Axial Strain $\epsilon_z = \epsilon_o$ ($h_1 = h_2 = h = 0.25$ in., $b/h = 8$, $a = 0.25$ in.).

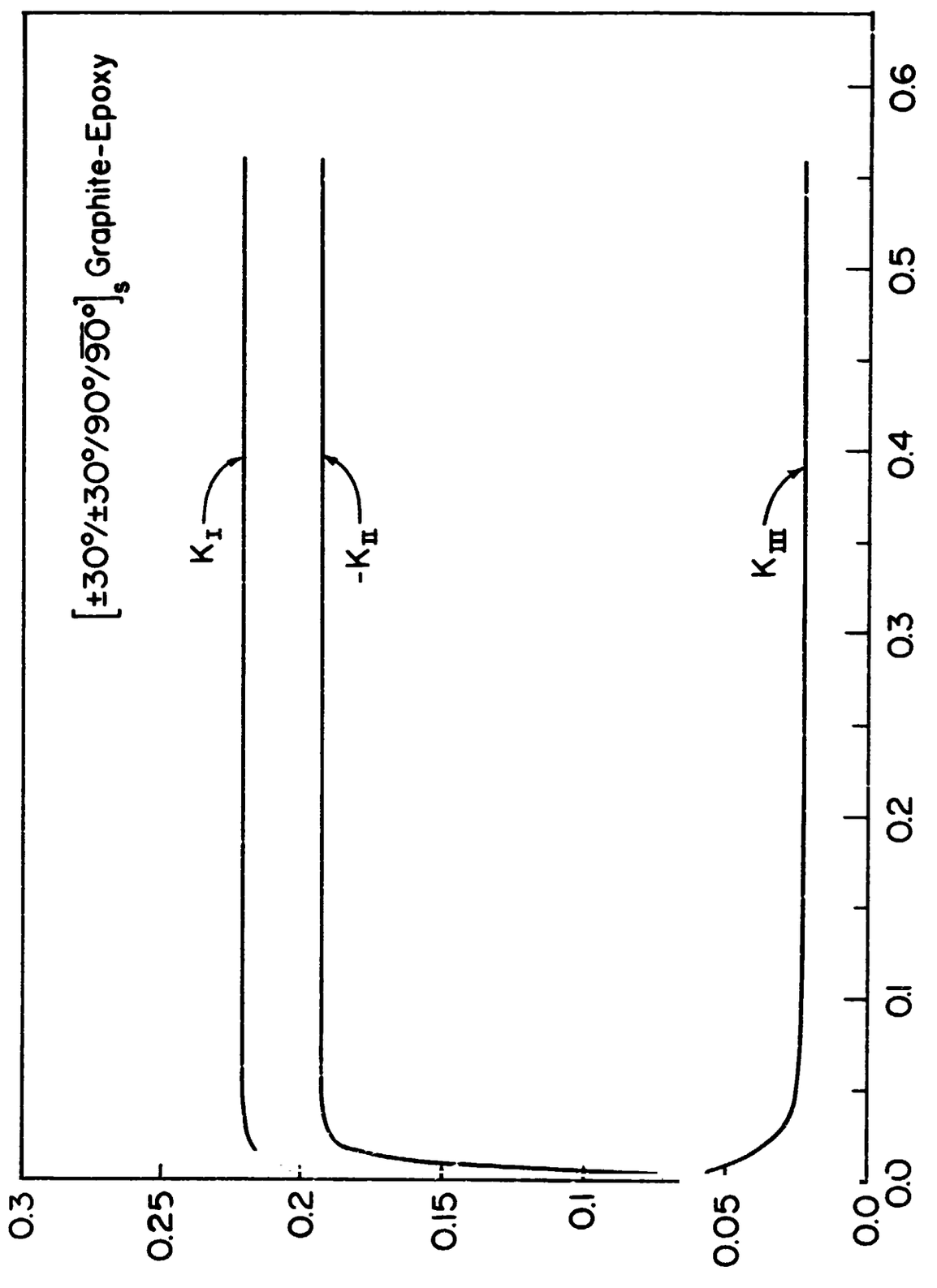

Fig. 12 Change of Stress Intensity Solutions K_i with Delamination Length a/b in $[(\pm 30°)/(\pm 30°)/90°/\overline{90°}]_s$ Graphite-Epoxy Subjected to Uniform Axial Strain $\epsilon_z = \epsilon_o$ ($h_1 = h_2 = \ldots = h_{11} = 0.0054$ in., $b = 0.75$ in.).

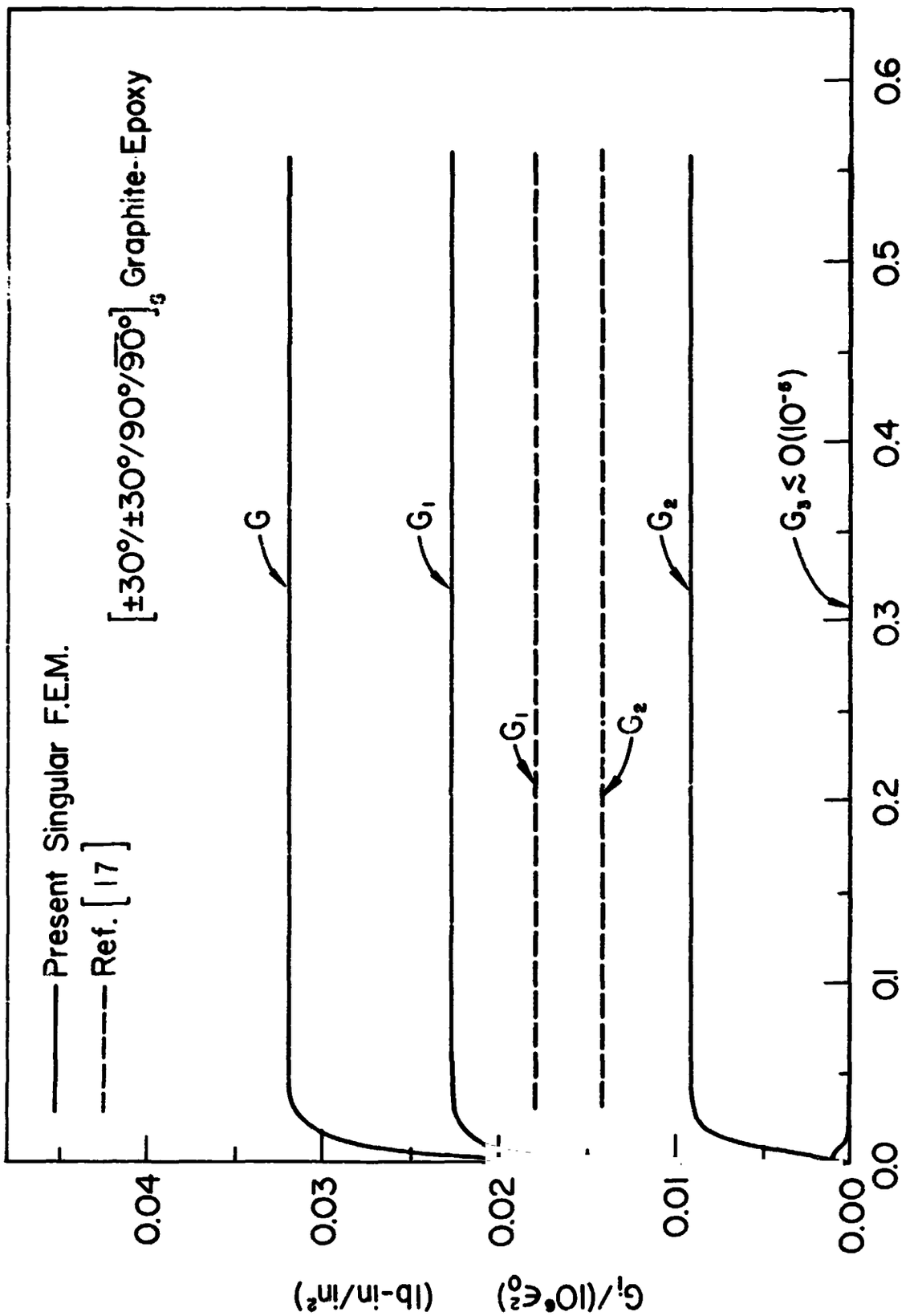

Fig. 13 Change of Strain Energy Release Rates G_i with Delamination Length a/b in $[(\pm 30°)/(\pm 30°)/90°/\overline{90°}]_s$ Graphite-Epoxy Subjected to Uniform Axial Strain $\varepsilon_z = \varepsilon_0$ ($h_1 = h_2 = \ldots = h_{11} = 0.0054$ in., $b = 0.75$ in.).

APPENDIX 1

Shape Functions $\underset{\sim}{N}_s(\rho,\xi;\delta)$ for the Singular Delamination Crack-Tip Element

Corresponding to a singular eigenvalue δ, the shape functions $\underset{\sim}{N}_s$ in local triangular polar coordinates (ρ,ξ) for the six-node conforming crack-tip element in the delamination problem are shown [4] to have the following expressions:

$$N_{ii} = 1 + [(2-2^{-\delta})\rho-\rho^{\delta+1}]/(2^{-\delta}-1), \tag{A1-1}$$

$$N_{i(3+i)} = 2^{-\delta}\rho(1-\xi)/(2^{-\delta}-1) - \rho^{\delta+1}[2\xi(1-\xi)+(1-\xi)/(2^{-\delta}-1)], \tag{A1-2}$$

$$N_{i(6+i)} = 2^{-\delta}\rho\xi/(2^{-\delta}-1) - \rho^{\delta+1}[2\xi(1-\xi)+\xi/(2^{-\delta}-1)], \tag{A1-3}$$

$$N_{i(9+i)} = - [2\rho(1-\xi)+2\rho^{\delta+1}(1-\xi)]/(2^{-\delta}-1), \tag{A1-4}$$

$$N_{i(12+i)} = 4\rho^{\delta+1}\xi(1-\xi), \tag{A1-5}$$

$$N_{i(15+i)} = - 2[\rho\xi-\rho^{\delta+i}\xi]/(2^{-\delta}-1), \qquad (i = 1,2,3), \tag{A1-6}$$

where the singular eigenvalues δ's are determined in accordance with the local crack-surface boundary conditions discussed in Section 2.1, and the ρ and ξ are related to the global coordinates by

$$\xi = \frac{(x_2-x_1)\tan\phi-(y_2-y_1)}{(y_3-y_2)-(x_3-x_2)\tan\phi}, \tag{A1-7}$$

$$\rho = r/f(\xi), \tag{A1-8}$$

in which

$$f(\xi) = \{(x_2-x_1)^2+(y_2-y_1)^2+2\xi[(x_2-x_1)(x_3-x_2)+(y_2-y_1)(y_3-y_2)] + \xi^2[(x_3-x_2)^2+(y_3-y_2)^2]\}^{1/2}. \tag{A1-9}$$

APPENDIX 2

Iteration Scheme for Partially Closed Delamination

For a delamination with crack surfaces in finite-length contact, the following iteration scheme is used for determining contact stress and crack closure length:

(i) Assume an initial contact length c_1, and solve Eq. 21 with the side conditions Eqs. 23(a) and 23(b) for contact stress and displacement.

(ii) Check the solution against preset criterion η_f. If the compressive stress $F_1 = \sigma_2(-c_1,\pi)$ gives a η_1 [$\eta_1 \equiv |(F_1-F_o)/F_o|$, and F_o is a properly selected sealing factor, for example, F_o is set as $10^6\ \varepsilon_o$ (psi), in the present calculation.] such that $\eta_1 < \eta_f$ and if the displacement field is admissible (i.e., no overlapping or interpenetration beyond the contact region), we set the crack closure length $c = c_1$ and terminate the iteration.

(iii) If the two constraint conditions are not met, a new contact length $c_2 > c_1$ is assumed and the procedure of (i) and (ii) is repeated for F_2 and u_2.

(iv) If $F_i < 0$ $(i = 1,2)$ and $|\eta_2| > |\eta_1| > \eta_f$, the next assumed length c_3 should be $c_3 < c_1$, and repeat (iii) and (iv).

(v) If either $F_i < 0$ and $|\eta_1| > |\eta_2| > \eta_f$ or $F_1F_2 < 0$ and $|\eta_i| > \varepsilon_f$, the next assumed contact length is set as

$$c_3 = c_2 + F_2(c_2-c_1)/(F_1-F_2). \qquad \text{(A2-1)}$$

The iteration from (i)-(iii) continues until sufficient accuracy is reached.

(vi) As the constraint conditions are satisfied and the difference between assumed contact lengths is $|c_{n+1}-c_n| < \varepsilon_c$, the iteration is terminated with $c = \frac{1}{2}|c_{n+1}+c_n|$.